

# Murine intestinal stem cells are highly sensitive to modulation of the T3/TR $\alpha$ 1-dependent pathway

Matthias Godart<sup>1</sup>, Carla Frau<sup>1</sup>, Diana Farhat<sup>1,\*</sup>, Maria Virginia Giolito<sup>1,\*</sup>, Catherine Jamard<sup>1</sup>, Clementine Le Nevé<sup>1</sup>, Jean-Noel Freund<sup>2</sup>, Luiz O. Penalva<sup>3</sup>, Maria Sirakov<sup>4</sup> and Michelina Plateroti<sup>1,\*‡</sup>

## ABSTRACT

The thyroid hormone T3 and its nuclear receptor TR $\alpha$ 1 control gut development and homeostasis through the modulation of intestinal crypt cell proliferation. Despite increasing data, in-depth analysis on their specific action on intestinal stem cells is lacking. By using *ex vivo* 3D organoid cultures and molecular approaches, we observed early responses to T3 involving the T3-metabolizing enzyme Dio1 and the transporter Mct10, accompanied by a complex response of stem cell- and progenitor-enriched genes. Interestingly, specific TR $\alpha$ 1 loss-of-function (inducible or constitutive) was responsible for low *ex vivo* organoid development and impaired stem cell activity. T3 treatment of animals *in vivo* not only confirmed the positive action of this hormone on crypt cell proliferation but also demonstrated its key action in modulating the number of stem cells, the expression of their specific markers and the commitment of progenitors into lineage-specific differentiation. In conclusion, T3 treatment or TR $\alpha$ 1 modulation has a rapid and strong effect on intestinal stem cells, broadening our perspectives in the study of T3/TR $\alpha$ 1-dependent signaling in these cells.

**KEY WORDS:** Intestinal stem cells, Organoids, Thyroid hormone, Thyroid hormone nuclear receptor

## INTRODUCTION

The intestinal epithelium is structurally and functionally organized in a monostratified cell layer that, along a vertical axis, defines the crypts of Lieberkühn and the villi (van der Flier and Clevers, 2009). At the bottom of the crypts are self-renewing multipotent stem cells (SCs) and their rapidly amplifying daughter cells (Barker, 2014; Umar, 2010). Progenitor cells differentiate during their migration to the apex of villi and acquire their differentiated properties, becoming secretory and absorptive cells (Noah et al., 2011). This regulation is tightly controlled, given that the entire intestinal epithelium is renewed every 4–5 days in mammals (van der Flier and Clevers, 2009). The balance between SC self-renewal, progenitor proliferation and differentiation commitment in the crypts depends on the cross-regulation of several signaling pathways including


Wnt, Hedgehog, Notch, BMP and thyroid hormones (Frau et al., 2017; Spit et al., 2018). In particular, Wnt and Notch activities are necessary for the maintenance of stem identity, and their dysregulation is a key determinant of cell differentiation engagement (Tian et al., 2015; van Es et al., 2005). It is worth noting that a high plasticity exists in the intestinal crypts and, in fact, different cell populations have been described, including the active SCs and cells with a potential to revert into an SC-like phenotype such as early progenitors or quiescent/slow cycling cells, also called reserve SCs (Gehart and Clevers, 2019; Li and Clevers, 2010). Active SCs expressing Lgr5 have been extensively studied and were identified as the cells responsible for continuous epithelial renewal (Barker et al., 2007), whereas the other SC-like populations including reserve SCs play a role in tissue repair upon injury and are mobilized following the loss of active SCs (Barker et al., 2010; Beumer and Clevers, 2016; Murata et al., 2020).

Importantly, we have previously demonstrated the key involvement of thyroid hormone (TH, namely T3 and T4)-induced signaling and TR $\alpha$ 1 (T3 nuclear receptor)-induced signaling in intestinal development and homeostasis, through the control of Wnt and Notch activities (Kress et al., 2009, 2010; Sirakov et al., 2015). TR $\alpha$ 1 is encoded by the *Thra* gene and it is the only bona fide T3 receptor transcribed by this gene that is able to bind both T3 and DNA (Brent, 2012). From a molecular point of view, thyroid hormone receptors (TRs) modulate the expression of target genes by binding to thyroid hormone response elements (TREs) present in regulatory regions of target genes. Upon T3 binding, TRs undergo a conformational change enabling activation or repression of the transcriptional machinery (Brent, 2012). TR $\alpha$ 1 is specifically expressed in intestinal crypt cells (Kress et al., 2009, 2010), in which it acts as a direct activator of Wnt (Kress et al., 2009; Plateroti et al., 2006) and Notch pathways (Sirakov et al., 2015), as well as of cell proliferation (Kress et al., 2009, 2010; Uchuya-Castillo et al., 2018). These data are consistent with the phenotype described in TR $\alpha$ -knockout animals or in TR $\alpha$ 1-overexpressing mice (Kress et al., 2009, 2010; Plateroti et al., 2001, 2006). The TR $\beta$ 1 receptor, encoded by the *Thrb* gene, presents an expression profile restricted to the differentiated epithelial cells of the villi (Sirakov et al., 2014) and no overt function for this protein has been described in the intestine (Plateroti et al., 1999).

Even though many studies have described the major involvement of THs in intestinal postnatal development during amphibian metamorphosis and in SC emergence (Frau et al., 2017; Ishizuya-Oka et al., 2009; Shi et al., 2011), specific investigations in mammals are lacking. In our study, we took advantage of a collection of TR $\alpha$ -mutated models as well as *Lgr5*-EGFP-IRES-CreERT2 mice (Barker et al., 2007) to specifically analyze the SC compartment and its response to T3-dependent signaling *in vivo* and in *ex vivo* 3D organoids. Cellular and molecular analyses enabled us to establish a specific action of T3 on intestinal SCs and the pivotal role of TR $\alpha$ 1 in this context.

<sup>1</sup>Centre de Recherche en Cancérologie de Lyon, INSERM U1052, CNRS UMR5286, Université de Lyon, Université Lyon 1, Centre Léon Bérard, Département de la recherche, 69000 Lyon, France. <sup>2</sup>Université de Strasbourg, Inserm, IRFAC/UMR-S1113, FMTS, 67200 Strasbourg, France. <sup>3</sup>Children's Cancer Research Institute, University of Texas Health Science Center at San Antonio, San Antonio, TX 78229, USA. <sup>4</sup>Department of Biology and Evolution of Marine Organisms, Stazione Zoologica Anton Dohrn, Villa Comunale, 80121 Napoli, Italy. <sup>\*</sup>Present address: Université de Strasbourg, Inserm, IRFAC/UMR-S1113, FMTS, 67200 Strasbourg, France.

<sup>‡</sup>Author for correspondence (michelina.plateroti@univ-lyon1.fr)

 M.V.G., 0000-0002-4888-7857; M.P., 0000-0003-0644-8837

Handling Editor: Gordon Keller  
Received 22 June 2020; Accepted 8 March 2021

## RESULTS

### Molecular action of T3 on *ex vivo* 3D organoids

Previous studies have underlined the importance of T3 on intestinal proliferation and regulation of key signaling pathways via its nuclear receptor TR $\alpha$ 1 both *in vivo* and in 2D primary cultures (Kress et al., 2009; Plateroti et al., 2006; Sirakov et al., 2015). We recently started employing in our research 3D primary intestinal epithelium organoid cultures, as they constitute an exquisite cellular *ex vivo* model to study SCs in the gut (Sato et al., 2009). We took advantage of this model, tested the response of organoids to 10<sup>-7</sup> M T3-containing medium, which appeared to be the appropriated concentration for our studies (Fig. S1) and performed a kinetic analysis of T3 treatment over 24 h (Fig. 1). Although we did not notice any difference from a morphological point of view (Fig. 1A), we observed a very early response in the expression of *Dio1* and *Mct10* (also known as *Slc16a10*) mRNAs, a T3-metabolic enzyme and a TH transporter, respectively (Bianco and da Conceição, 2018; Groeneweg et al., 2017), which displayed significant upregulation in T3-treated organoids following 3 h of treatment (Fig. 1B). The T3-direct target gene *Jag1* was also upregulated upon T3 treatment (Fig. 1B), further confirming the efficacy of the treatment. Cyclin D1 (*Ccnd1*) was also upregulated after several hours of T3-treatment and remained significantly upregulated until the end of the experimental time-course (Fig. 1B), suggesting a positive regulation of cell proliferation. To verify this assumption, we performed EdU incorporation analysis and revealed proliferating cells by EdU labeling after 10 h and 24 h of T3 treatment. Although there was only a slight difference between control and T3 treatment at 10 h, at 24 h some organoids treated with T3 displayed an increased size and longer buddings where Edu-related proliferation was specifically restricted (Fig. 1C). Surprisingly, when we focused on the expression of SC markers we observed a complex scenario (Fig. 1B) with classical markers of active SCs such as *Lgr5*, *Olfm4* and *Ascl2* mRNA being significantly decreased in T3-treated organoids at 24 h. In parallel, markers considered to characterize facultative SCs, namely *Msi1*, *mTert* (*Tert*) and *Hopx* mRNAs were marginally or not affected (Fig. 1B). Of note, T3 treatment did not affect the expression of SC genes, proliferation-related markers or EdU labeling in TR $\alpha$ <sup>0/0</sup> organoid cultures. *Dio1* and *Mct10* mRNAs were upregulated by T3 at later time points, possibly through TR $\beta$ 1 (Amma et al., 2001) (Fig. S2).

Because of the intriguing results on SC markers, we then decided to perform a global analysis of RNA-seq on organoids maintained in control conditions or treated with T3 for 17 h, a time-point at which morphology remains unaffected but the molecular response to the hormone is clearly visible. We used statistical approaches to identify significant differentially expressed genes (DEGs) and retained only the genes presenting a log<sub>2</sub> fold change  $\geq \pm 0.5$  and a *P*-value  $< 0.05$  (Table S1). The hierarchical clustering clearly grouped the genes according to culture conditions (Fig. 2A). Gene ontology (GO) analysis identified stress response and metabolism among the most relevant enriched biological functions (Fig. 2B,D). Molecular pathways that were significantly represented within the DEGs included retinoic acid signaling and xenobiotics (downregulated) as well as Toll-like receptor cascade and various transporter types (upregulated) (Fig. 2C,E). We also performed gene set enrichment analysis (GSEA) to compare our DEGs with genes preferentially expressed in SCs or in progenitor cells (Fig. 3A; Tables S2 and S3). The upregulated genes of our analysis were more significantly associated with a progenitor-type molecular signature (Fig. 3B; Fig. S3A; Tables S2 and S3), whereas the downregulated genes were more significantly associated with an SC molecular signature

(Fig. 3C; Fig. S3B; Table S2). Bioinformatics analysis also revealed a network of functionally linked downregulated genes encoding SC markers and/or linked to SC biology (Fig. 3D). It is worth noting, however, that the molecular repertoire induced or repressed by T3 in organoids appears to be complex. Indeed, among upregulated genes associated with the SC signature, we observed the presence of the *Clu* (clusterin) gene (Fig. 3E; Table S2), which has recently been associated with a population of slow cycling/quiescent/revival intestinal SCs (Ayyaz et al., 2019). This suggests that an action on active SCs might be counterbalanced by a possible induction of a new population of SCs. In addition, this category of genes includes signaling molecules (*Tlr2*), genes involved in apoptosis (*Casp12*) or in molecule/ion transport (*Slc14a1*, *Slco3a1* and *Kcne3*). Among upregulated genes associated with a progenitor signature, we denoted proteins involved in retinol (*Rbp7*), TGF $\beta$ /BMP (*Tgfb1*) or Wnt (*Epha2*) signaling. Finally, we compared our dataset to DEGs described in laser microdissected crypts from pre-weaned TH-treated or untreated mice (Kress et al., 2009) (Table S4). Interestingly, a strong overlap of the two lists of DEGs was unveiled, which included several metabolism-linked genes, the proto-oncogene *cFos* (*Fos*), *Klf9*, a well-known direct T3-target gene (Denver and Williamson, 2009), and signaling molecules. Furthermore, three genes were inversely regulated by T3 in organoids in comparison with crypts, namely *Fgfl*, *Gcnt2* and *Notch1*, which are involved in cell signaling, cell fate and regulation of mucin expression, respectively (Chen et al., 2009; Danopoulos et al., 2017; Siebel and Lendahl, 2017).

This molecular analysis and comparison with previous studies indicate that 17 h of T3 treatment induces a ‘thyroid shock’ in organoids through a complex response that includes stress response, metabolic challenge and alteration of cell signaling. In addition, we identified a molecular signature of early T3-induced events, some of which displayed a clear overlap with previously described genes in intestinal crypts *in vivo*.

### Growth characteristics of organoids upon T3 treatment

The previous results compelled us to investigate the effect of T3 on the kinetics of 3D organoid development and structuration (i.e. increasing size and number of buds) over time. We used *Lgr5*-EGFP-IRES-Cre<sup>ERT2</sup> (hereafter designated as *Lgr5*-EGFP) mice in order to highlight and visualize *Lgr5*-expressing SCs (Barker et al., 2007). Freshly prepared crypts were cultured in control and 10<sup>-7</sup> M T3-containing medium. As expected, we observed an increase in organoids displaying an augmented structural complexity in control condition, as illustrated by the growing size and number of buds appearing over time and a concomitant decrease in simple structured organoids (Fig. 4A,B; Fig. S4A). In T3-treated organoids, a multi-phasic response took place. First, we observed a decrease in the rate of spheres at day (D) 1 and D2 in parallel with the induction of complex structure formation (1-2 buds or more than 2 buds) until D3. This was followed by an almost stable percentage of less-complex organoids (1-2 buds) or their loss (more than 2 buds) after D3 (Fig. 4B; Fig. S4A). When we further analyzed the effects induced by T3 on organoids, we observed a change of morphology clearly visible from D4 onwards, with organoids displaying a larger central body and a decreased number of buds (Fig. 4A). Quantification of these parameters confirmed a significant increase in the central body in T3-treated compared with untreated organoids from D2 onwards. The number of buds significantly increased at D1, was unchanged at D2 but decreased at D3 and D4, whereas the total surface of the organoids showed no significant difference from control and T3 conditions at all time points analyzed (Fig. S4B). The growth of the organoids was



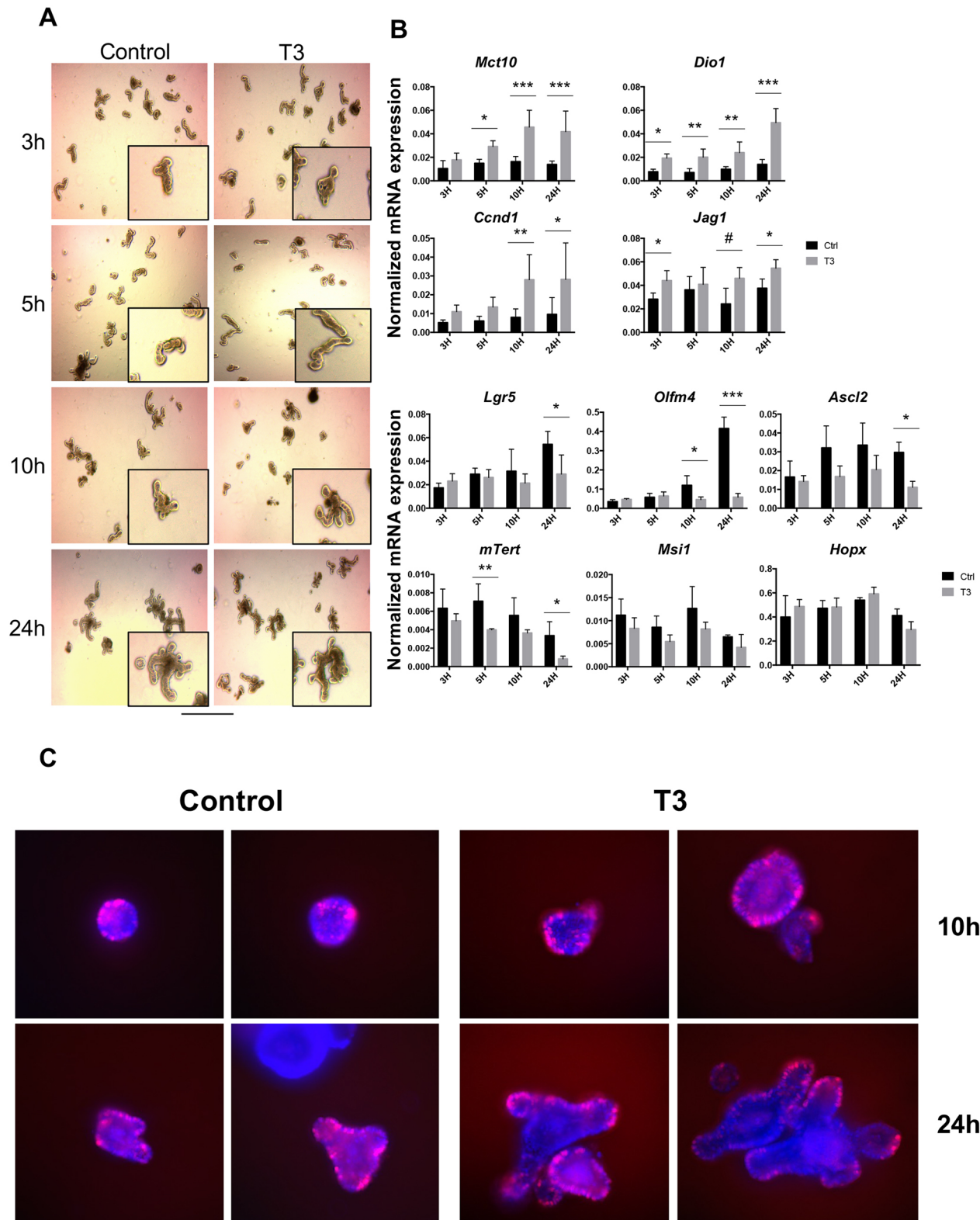


**Fig. 1. Short-term response of organoids to T3.** (A) Replicated wild-type organoids were cultured over 24 h in the absence (Control) or presence of  $10^{-7}$  M T3, as indicated. The pictures were taken at different time points and are representative of three independent experiments, each conducted on six replicates. Insets show high magnification area of main image. (B) RT-qPCR experiments were performed at different time points, as indicated, to analyze the mRNA expression of the TH metabolizing enzyme *Dio1* and transporter *Mct10*; *Ccnd1* was used as a proliferative marker and *Jag1* as a direct T3-target gene. In addition, stem cell markers *Lgr5*, *Olfm4*, *Ascl2*, *mTert*, *Msi1* and *Hopx* were also analyzed. Histograms represent mean $\pm$ s.d.,  $n=4$ , after normalization with *Ppib*. \* $P<0.05$ , \*\* $P<0.01$ , \*\*\* $P<0.001$  compared with the respective control conditions. # indicates marginally significant ( $P=0.071$ ) compared with the respective control conditions. (C) Proliferation analysis by EdU incorporation on organoids in the control condition or treated with T3 for 10 h or 24 h; in both cases EdU was added in the culture medium 2 h before ending the cultures. Images show merged EdU labeling (red) and nuclear staining (blue). Scale bars: 30  $\mu$ m (A); 15  $\mu$ m (A, insets); 7  $\mu$ m (C).

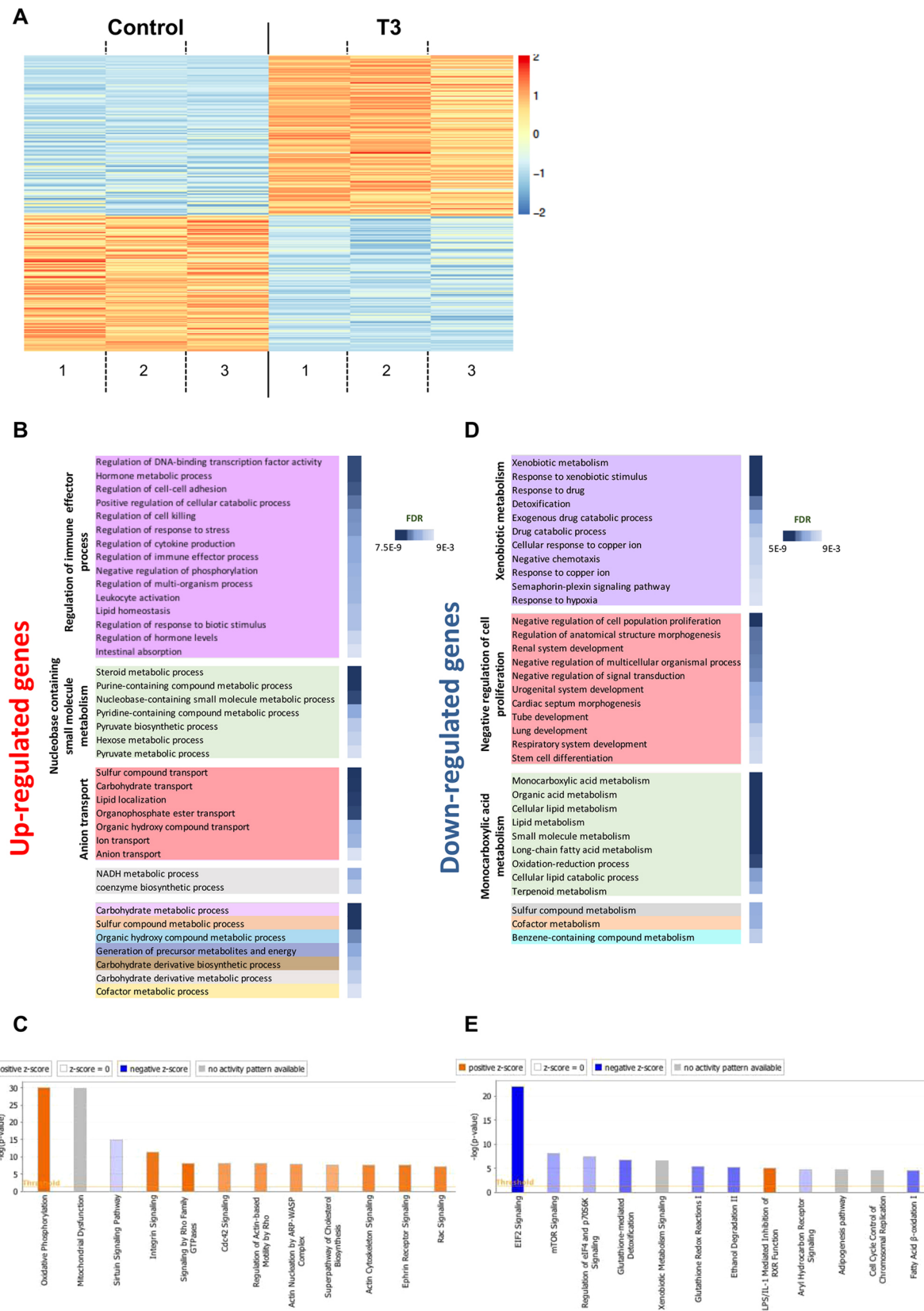


**Fig. 2. Comparative transcription profile analysis of T3-treated organoids by RNA-seq.** (A) Hierarchical clustering after RNA-seq enabled observation of the links between the organoid cultures in T3 or control conditions and to visualization of differentially expressed genes. In this clustering, the transcripts were grouped in two dendrograms, each of which represents a condition. Each line is a gene and each column is an RNA sample. Expression signal intensities are shown in red and blue, indicating high and low expression levels, respectively. (B,D) Gene Ontology (GO) terms enriched among genes showing increased (B) or decreased (D) expression upon T3 treatment. GO enriched terms are summarized using REViGO (Supek et al., 2011). (C,E) Ingenuity Pathway Analysis: bar charts show the most significant canonical pathways associated with the differentially-expressed increased (C) or decreased (E) genes.

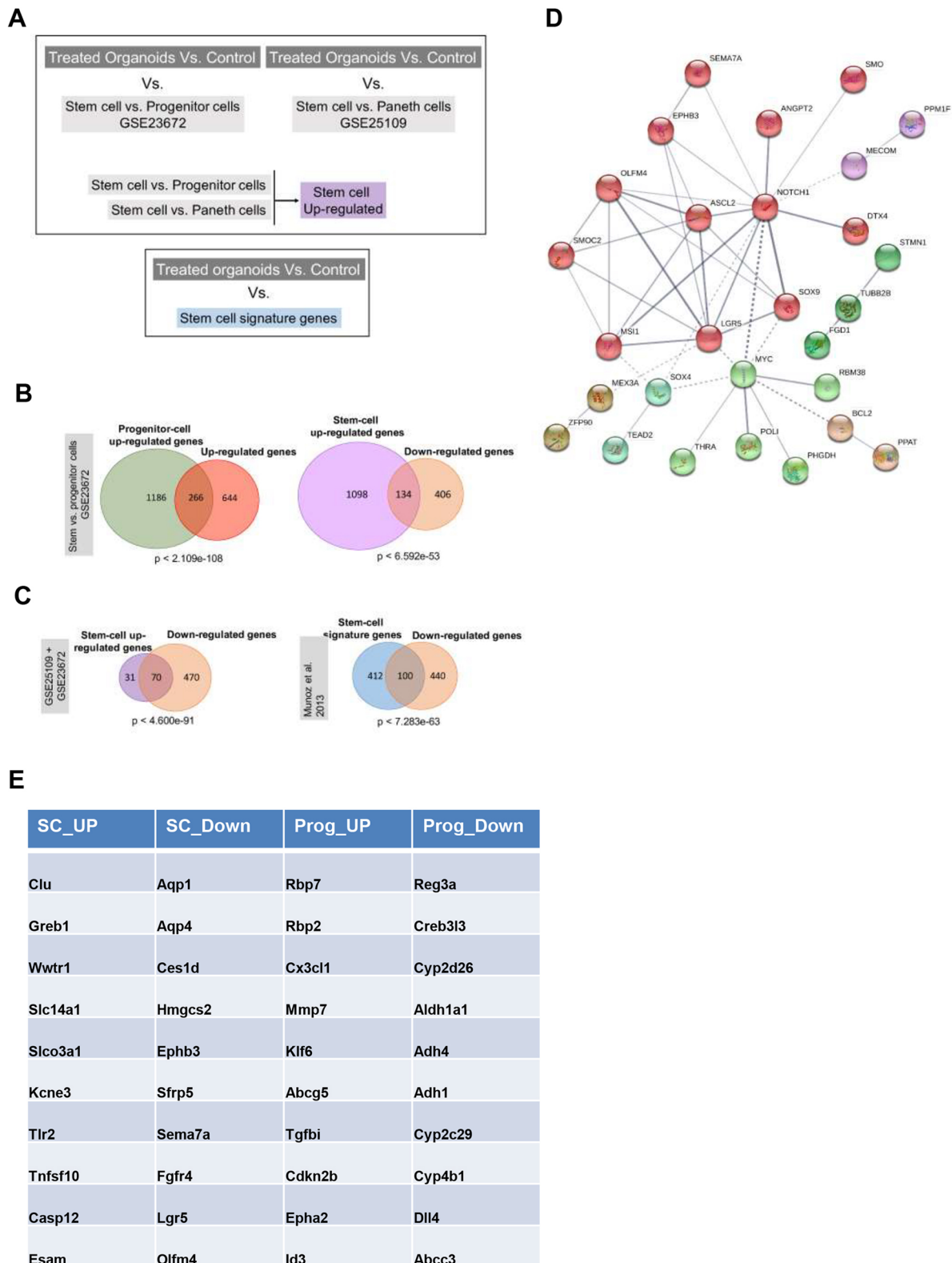


**Fig. 3. Differentially-expressed genes and molecular signatures of intestinal crypt cell populations.** (A) Diagram showing the comparison between different datasets to evaluate the changes in expression induced by T3 treatment. (B) Venn diagrams showing the overlaps between our dataset and GSE23672. The upregulated set in our analysis encompasses a large number of genes highly expressed in progenitor cells, whereas the downregulated set is similar to the gene set expressed in stem cells. (C) Venn diagrams showing the comparison between downregulated genes in our dataset and the 'stem cell' signatures. Hypergeometric test was conducted to define the significance of the overlap between groups. *P*-values show significance of overlap based on the number of expressed and altered genes. (D) Network of stem cell-related genes present in the downregulated set. Analysis was performed using String. Each colored cluster is defined by proteins (genes) showing strong functional associations between them. (E) Examples of genes up- or downregulated in our analysis associated with stem cell or progenitor signatures.



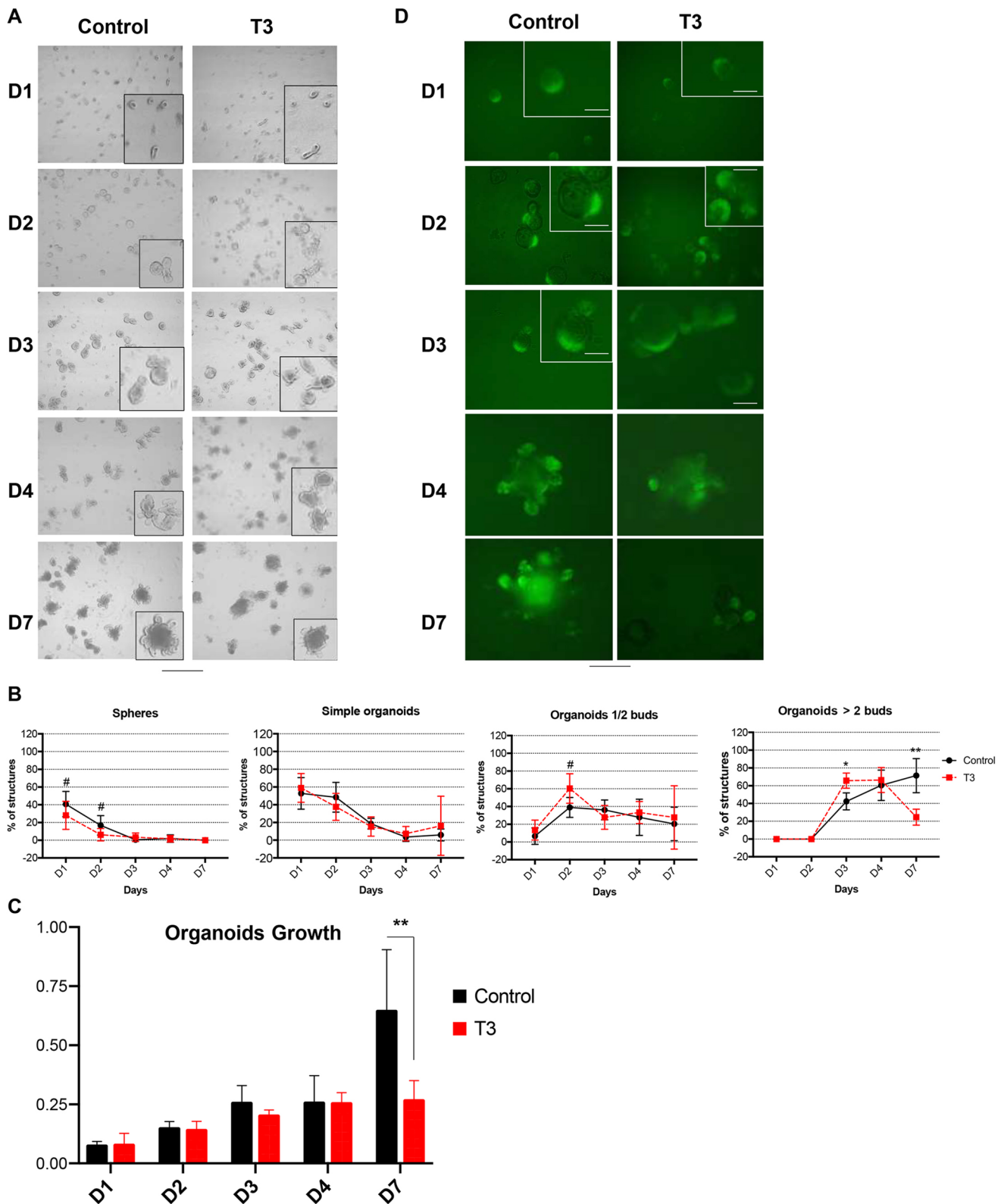


**Fig. 4. Analysis of growth properties and features of cultured crypts.** (A) Crypts were prepared from *Lgr5*-EGFP intestine and maintained in culture for several days in the absence (Control) or presence of  $10^{-7}$  M T3 as indicated, allowing complex organoid development with increased number of buddings. Pictures were taken under an inverted microscope at the indicated days, and are representative of three/four independent experiments. (B) Graphs show the percentage of spheres, simple organoids, 1-2 bud organoids and more complex organoids (>2 buds) evaluated every day for 1 week.  $n=6$ . (C) Growth of organoids over time in culture, in control or T3 condition as indicated, analyzed using the WST-1 assay.  $n=12$ . (D) Live GFP fluorescence analysis of fresh *Lgr5*-EGFP organoids cultured in the presence or absence of T3 at indicated days in culture. Data are mean $\pm$ s.d. \* $P<0.05$ , \*\* $P<0.01$  compared with the respective control conditions. #, marginally significant (spheres D1,  $P=0.052$ ; spheres D2,  $P=0.061$ ; organoids 1/2 buds D2,  $P=0.06$ ) compared with the respective control conditions. D, days in culture. Scale bars: 30  $\mu$ m (A); 15  $\mu$ m (A, insets); 10  $\mu$ m (D); 5  $\mu$ m (D, inset).

also monitored using the WST-1 Assay Reagent that quantifies cell proliferation and viability. Organoids treated with T3 at different time points showed a profile similar to that of the development of complex organoids, with a decreased growth at D7 compared with the respective untreated condition (Fig. 4C). Live fluorescence microscopy revealed GFP-positive cells from D1 to D7 in both control and T3 conditions (Fig. 4D). It is worth noting that from D1 to D3 the T3-treated organoids displayed more bud-like structures with a high number of GFP-positive cells (Fig. 4D). After a longer treatment time, we detected a clear decrease in both GFP intensity and GFP-positive cells (Fig. 4D, panel D7).

A parallel analysis of cell proliferation and cell death by immunofluorescence (IF) indicated a different patterning of KI67-positive cells at D2 compared with control organoids (Fig. 5A). Indeed, although in controls the proliferating cells were spread across the organoids (central and peripheral parts), in the T3-treated condition organoids presented a more evident zonal organization, with KI67-positive cells located within the emerging buds (Fig. 5A). These qualitative observations were confirmed by quantifying KI67-positive cells within the buds or outside the buds in both conditions (Fig. 5B). At D4, the control organoids had KI67-positive cells within the crypt-like structures, whereas this zone appeared to be reduced in the T3-treated condition (Fig. 5A). Indeed, the number of KI67-positive cells was more abundant in the buds in both conditions but it was significantly decreased in T3-treated organoids (Fig. 5B). Western blot (WB) analysis revealed that the levels of phospho-Histone H3, an indicator of actively cycling cells (Kim et al., 2017; Nielsen et al., 2013), were unchanged at D2 but reduced at D4 (Fig. 5C). Concomitantly, we observed that in the T3 condition, apoptosis increased at both time points as visualized by cleaved-caspase 3-positive cells within the lumen by IF (Fig. 5A) and by WB (Fig. 5C). The analysis of differentiation markers indicated no changes in the number of enterocytes, enteroendocrine and Paneth cells (Fig. 5D), but we saw a significant increase in mucus-producing goblet cells (Fig. 5E). Several markers of TH metabolism, cell proliferation and of SCs were also analyzed at the mRNA level, further supporting the overall phenotype induced by T3 (Fig. S5). Finally, to confirm that the T3 phenotype specifically depended on T3 and not on other hormones/metabolites or integrins (Davis et al., 2011; Hammes and Davis, 2015; Kalyanaraman et al., 2014), we also performed experiments by treating the organoids with T4, 3,3'-T2 (derived from degradation of T3 or T4) and Tetrac (an inhibitor of T3 or T4 binding to integrins). However, only T4 could recapitulate the T3 phenotype (Fig. S6), as expected by the presence and expression pattern of *Dio1* in the organoids and its action in metabolizing T4 to T3 (Bianco and da Conceição, 2018).

Taken together, these data show an advanced appearance of buddings in organoids upon T3 treatment during development *ex vivo*, indicating an accelerated turnover. The accelerated turnover, however, is responsible for a loss of SC and their engagement in secretory differentiation, in particular towards the goblet lineage.

### The expression of a dominant negative TR $\alpha$ 1 strongly affects organoid growth *ex vivo*

TR $\alpha$ 1 has been shown to play a pivotal role in the intestinal crypt pathophysiology (Bao et al., 2019; Sirakov and Plateroti, 2011; Uchuya-Castillo et al., 2018). Using TR $\alpha$ 1<sup>L400R</sup> mice (hereafter designated as TRami), corresponding to a model of TR $\alpha$ 1 loss-of-function (Quignodon et al., 2007), we analyzed the effects of inducing the TR $\alpha$ 1 mutation on *ex vivo* 3D organoid growth and structuration. TRami animals were crossed with *Lgr5-EGFP* and *Rosa26/CAG-*

floxed-STOP-tdTomato mice (hereafter named *Rosa-Tomato*) (Madisen et al., 2010) to generate tamoxifen-inducible triple transgenic TRami/*Lgr5-EGFP/Rosa-Tomato* animals, in which loss of TR $\alpha$ 1 activity and expression of the Tomato fluorescent protein can be specifically induced in *Lgr5*-expressing crypt cells. Tamoxifen or corn oil (negative control) were injected *in vivo* into TRami/*Lgr5-EGFP/Rosa-Tomato* triple-transgenic animals and the intestine was recovered to perform crypt cultures and analyze organoid growth over time. The efficacy of the induction of the TRami allele by tamoxifen was validated by PCR on genomic DNA (Fig. S7A,B); no effect of tamoxifen was observed in TRami/*Lgr5-WT* organoids not expressing the inducible CRE protein (not shown). Live fluorescence microscopy confirmed the presence of double positive Tomato/GFP cells specifically in organoids from tamoxifen-injected mice compared with oil-injected control animals (Fig. S8A). As expected, organoids developed better in the oil/control condition, as evidenced by an increase in the number of organoids displaying several buds, a decrease in simple structured organoids (Fig. 6A,B) and the increased number of buds per organoid over the time in culture (Fig. 6C). Conversely, cultures from tamoxifen-induced TRami mice displayed a strong impairment in complex organoid formation (>2 buds) (Fig. 6A-C). Indeed, in this condition, most organoids remained at the stage of simple organoids or of organoids with 1-2 buds (Fig. 6B) and the number of buds per organoid was significantly decreased (Fig. 6C), strongly reflecting a negative impact of TRami induction on cell proliferation and eventually on SCs. Collectively, the expression of the dominant negative TR $\alpha$ 1 specifically in *Lgr5*-expressing cells definitely demonstrated a key role for this nuclear receptor in intestinal progenitor and SC physiology.

### Constitutive lack of TR $\alpha$ but not of TR $\beta$ decreases SC activity

Next, we further investigated intestinal SC activity depending on TR $\alpha$ 1 expression and decided to use a constitutive knockout model. Indeed, in this model cells do not express TR $\alpha$ 1, whereas in inducible models mosaic CRE expression (Barker et al., 2007) or inefficient recombination cannot be ruled out. We initially prepared fresh crypts from wild-type (WT) or TR $\alpha$ <sup>0/0</sup> animals and followed the kinetics of 3D organoid development and structuration over 7 days in culture (Fig. 7A-C). In WT cultures, we observed an increase in organoids displaying several buds and a concomitant decrease in simple structured organoids over the time-course of the experiment (Fig. 7A-C). TR $\alpha$ <sup>0/0</sup> crypt cultures showed a delay in development, whereas their growth profile indicated that simple structures were maintained for a longer period, with complex organoids forming more slowly (Fig. 7A-C). We also analyzed the number of buds per organoid at different time-points and observed that TR $\alpha$ <sup>0/0</sup> organoids presented a significantly lower number of buds at D4 and D7 compared with WT organoids (Fig. 7D). These phenotypes were specifically linked to TR $\alpha$ 1, as experiments in TR $\beta$ <sup>-/-</sup> crypt cultures revealed results similar to those of WT cultures (Fig. 7A-D). This observation is not surprising given that *Thra* but not *Thrb* mRNA expression is enriched in SCs (Table S5). Finally, T3-treatment experiments in TR $\alpha$ <sup>0/0</sup> and TR $\beta$ <sup>-/-</sup> organoids validated the specific involvement of TR $\alpha$ 1 (Fig. S9).

To further link the TR $\alpha$ 1-dependent phenotype to stemness we then measured colony-forming efficacy, which represents the ability of SCs to self-renew and generate organoids at the single cell level (Sato et al., 2009; Yin et al., 2014). Before conducting colony-forming assays, we cultured WT or TR $\alpha$ <sup>0/0</sup> organoids for 2 days and then dissociated and recovered the single cells from each genotype. We then seeded 5000 cells per well and cultured organoids over 7 days. At D7 we counted the number of colonies formed in TR $\alpha$ <sup>0/0</sup>

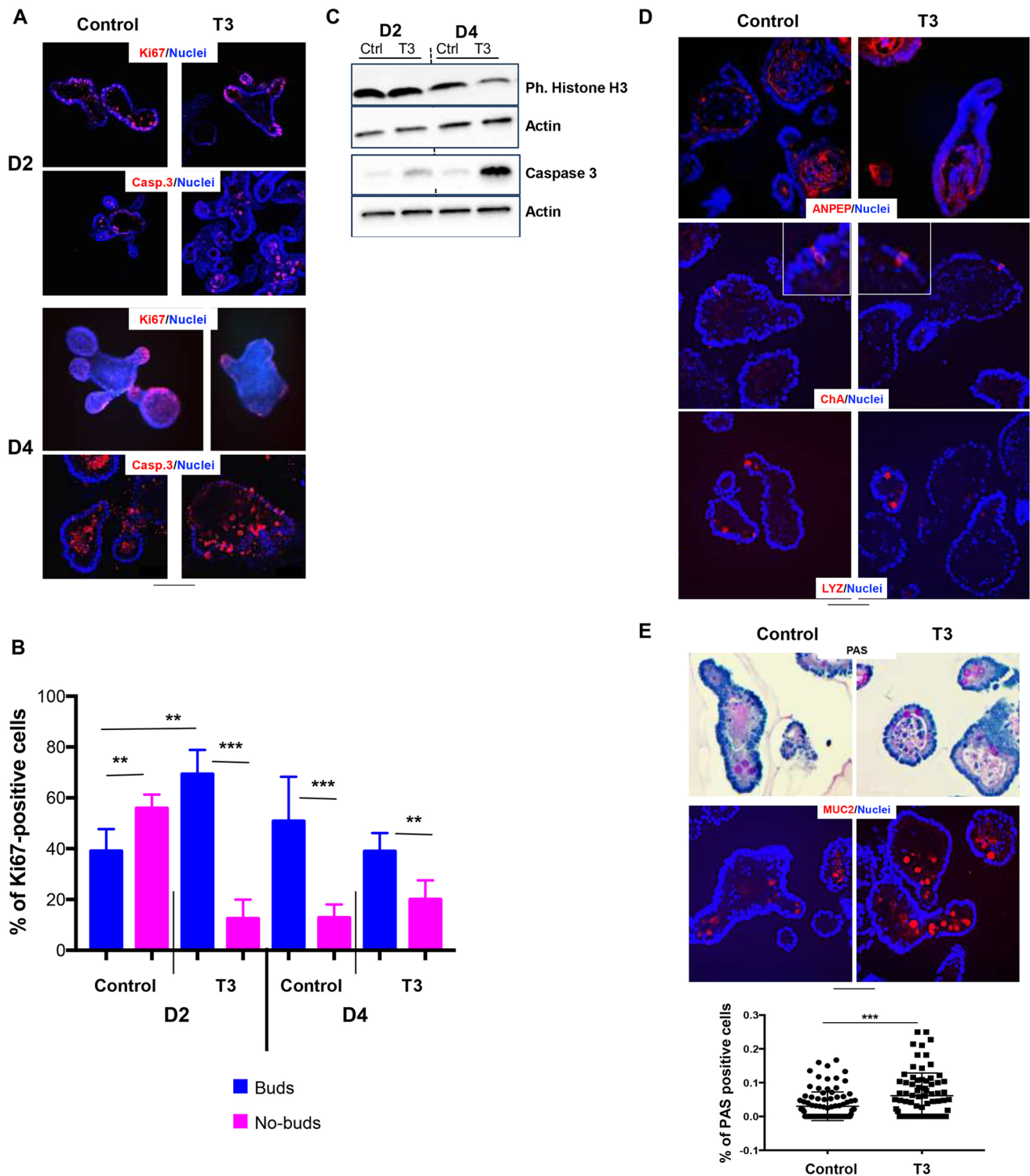


**Fig. 5. Accelerated turnover and unbalanced differentiation in T3-treated organoids.** (A) Ki67 and cleaved-caspase 3 immunolabeling of proliferating or apoptotic cells in organoids in control or T3 condition at day (D) 2 and D4. Images show merged specific immunolabeling (red) and nuclear staining (blue). Pictures are representative of three independent experiments. (B) Quantification of Ki67-positive cells in portions of organoids with buds or no-buds at D2 and D4 in control and T3-treated conditions, as indicated. (C) Western blot analysis of Histone H3, cleaved-caspase 3 levels in organoids in control or T3 condition at D2 and D4. Actin was used as the loading control. Pictures are representative of two independent experiments. (D) Analysis of differentiation markers in organoid paraffin sections in control or T3-treated conditions, as indicated, at D4. ANPEP (enterocytes), lysozyme (LYZ, Paneth cells) and chromogranin A (ChA, enteroendocrine cells) were analyzed by immunolabeling. The images show merged differentiation marker (red) and nuclear staining (blue). Pictures are representative of three independent experiments. (E) Analysis of mucus-producing goblet cell differentiation in organoids maintained in control or T3 conditions at D4. Upper panel shows mucus-producing cells stained with PAS or by immunolabeling with anti-MUC2 antibodies. Images show merged MUC2 (red) and nuclear staining (blue). Histograms in the lower panel summarize the quantification of PAS-positive cells in organoids depending on the culture condition. Approximately 50 organoids per condition were scored from pictures using the ImageJ software. Data are mean $\pm$ s.d. \*\* $P$ <0.01, \*\*\* $P$ <0.001 compared to indicated conditions. D, days in culture. Scale bars: 20  $\mu$ m (A); 10  $\mu$ m (D,E); 5  $\mu$ m (D, inset).



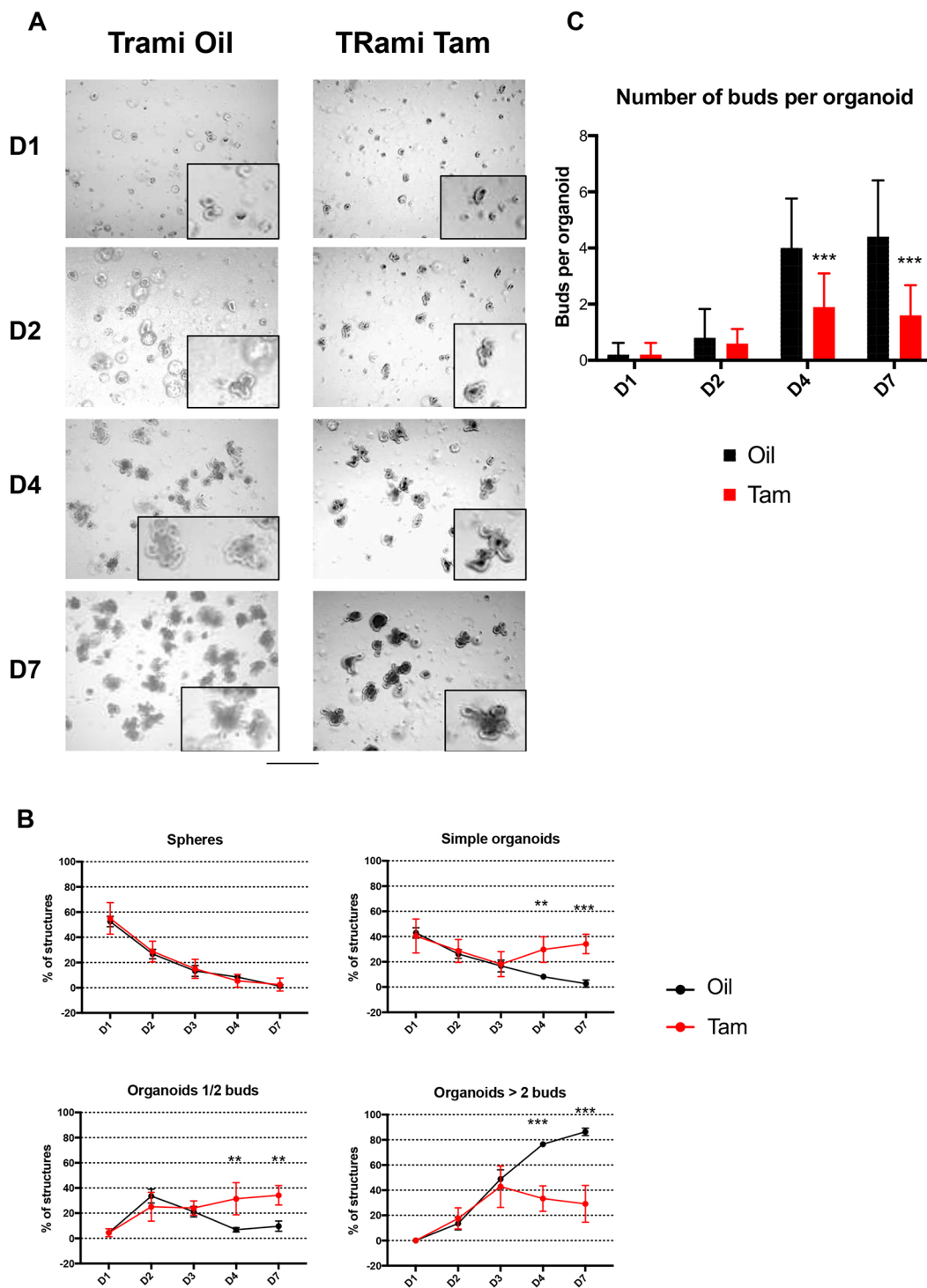


**Fig. 6. Inducible dominant negative TR $\alpha$ 1 expression has a negative effect on organoid development and structuration.** (A) Time-course of fresh crypts isolated from TRami/Lgr5-EGFP/Rosa-Tomato injected with oil or tamoxifen (Tam) before sacrifice, as indicated. Crypts were cultured and developing structures were observed at day (D) 1, D2, D4 and D7 of culture. Pictures are representative of two independent experiments. The insets focus on representative organoids from each condition. (B) The number of simple structure (spheres) or organoids of increasing complexity (1 or 2 buds, more than 2 buds) were scored under the inverted microscope over 7 days of culture.  $n=6$ . (C) The number of buds per organoid were scored at different time points in the control and T3 condition.  $n=20$ . Data are mean $\pm$ s.d. \*\* $P<0.01$ , \*\*\* $P<0.001$ . D, days in culture. Scale bars: 30  $\mu$ m (A); 15  $\mu$ m (A, insets).

compared with WT organoid cultures (Fig. 8A,B). As expected from *ex vivo* organoid developmental studies, TR $\alpha^{0/0}$  dissociated cultures had a strongly impaired capacity to generate new organoids, whereas no distinct phenotype was detected in TR $\beta^{-/-}$  colonies compared with WT cultures (Fig. 8A,B).

#### Impact of T3 on intestinal crypts *in vivo*

After defining the impact of T3 on intestinal SC biology in *ex vivo* organoids, we further characterized the relevance of our observations *in vivo*. For this aim, we treated Lgr5-EGFP animals with T3 *in vivo* and recovered the intestine 2 days after treatment. We analyzed the

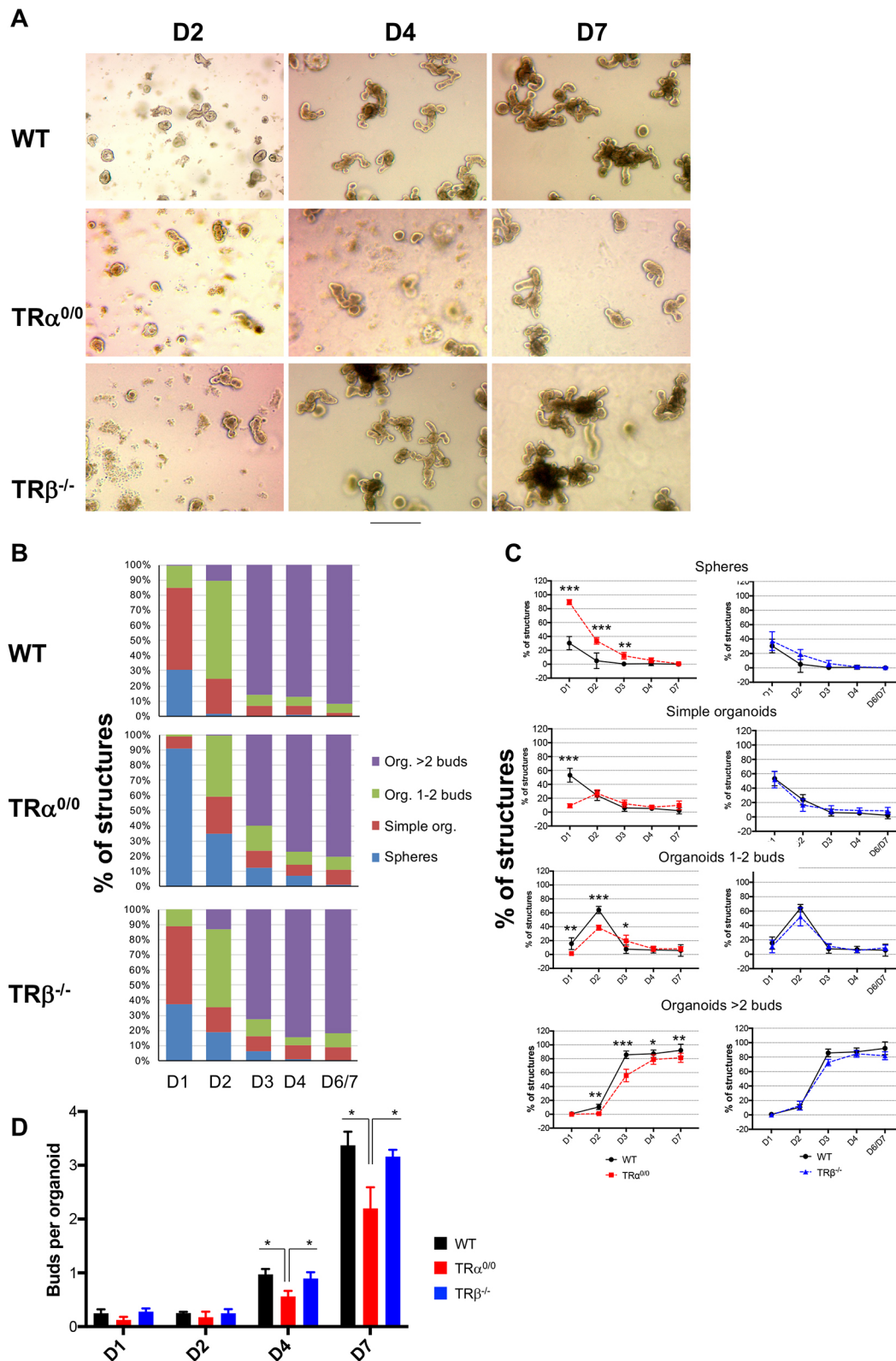


**Fig. 7. Specific TR $\alpha$ -dependent action on organoid development.** (A) Crypts were prepared from wild-type (WT), TR $\alpha^{0/0}$  and TR $\beta^{-/-}$  intestines and maintained in culture for several days, allowing complex organoid development. Pictures were taken under an inverted microscope at the indicated days, and are representative of three independent experiments. (B,C) Multilayered histograms (B) and graph lines (C) represent the mean $\pm$ s.d.,  $n=6$ , of each structure counted in the cultures from different genotypes. The number of simple structures (spheres) or organoids of increasing complexity (1 or 2 buds, more than 2 buds) were scored under the inverted microscope during 7 days of culture. \* $P<0.05$ , \*\* $P<0.01$ , \*\*\* $P<0.001$ . (D) The number of buddings per organoid was scored at key time points in cultured organoids of different genotypes. Histograms represent mean $\pm$ s.d.,  $n=20$ . \* $P<0.05$  compared with WT and TR $\beta^{-/-}$  organoids. D, days in culture. Scale bar: 15  $\mu$ m.

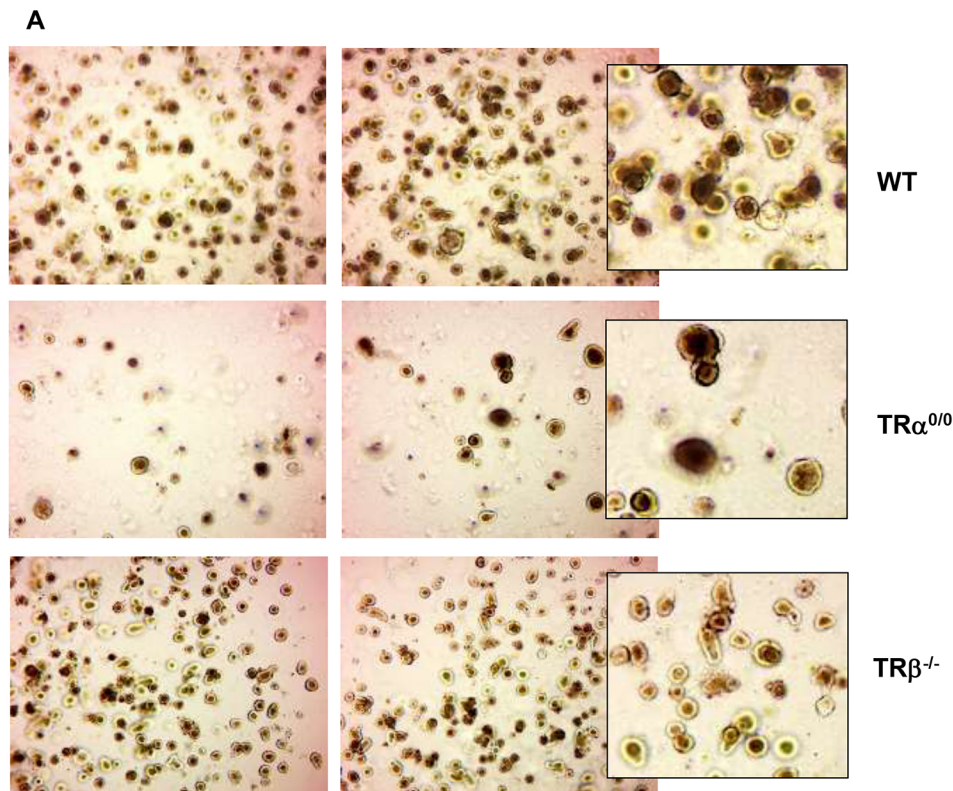
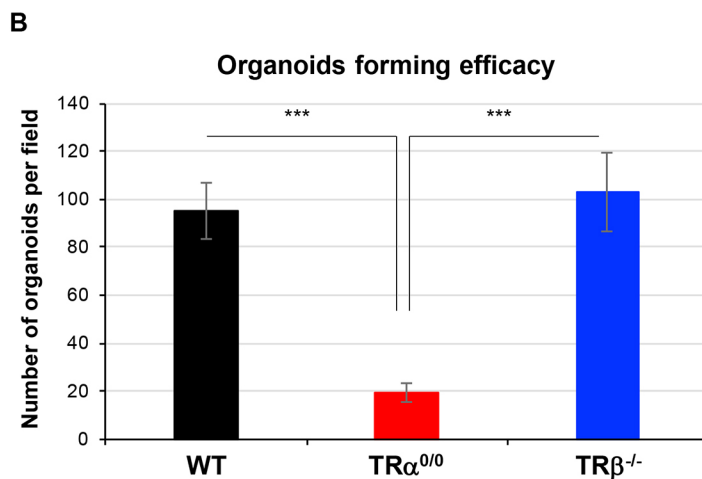


**Fig. 8. Lack of TR $\alpha$ 1 specifically affects stem cell activity.** (A,B) Colony assay was performed on single cells dissociated from organoids and maintained for 2 days in culture. Then 5000 cells prepared from wild-type (WT), TR $\alpha^{0/0}$  or TR $\beta^{-/-}$  organoids were cultured in Matrigel. Pictures in A were taken on day 7. Pictures are representative of two independent experiments each conducted in four replicates. Histograms in B show the number of colonies formed in each condition after 7 days in culture. Data are mean $\pm$ s.d.,  $n=4$ . \*\*\* $P<0.001$ . TR $\alpha^{0/0}$  compared to WT or TR $\beta^{-/-}$ . Scale bar: 15  $\mu$ m (A); 7  $\mu$ m (A, insets).



proliferative and differentiation properties of the intestine by IF on sections. As expected from our previous studies (Kress et al., 2009; Plateroti et al., 2006), T3 treatment induced an increase in the number of PCNA-positive proliferating crypt cells (Fig. 9A). The analysis of differentiation markers indicated that T3 injection did not lead to an overt difference between T3-treated and untreated animals regarding enterocytes, enteroendocrine cells or mucus-producing goblet cells (Fig. 9B), whereas Paneth cells were significantly increased in T3-treated intestine (Fig. 9B). We also analyzed the GFP-positive or OLFM4-positive SCs in these same conditions by IF (Fig. 10A) and observed an expansion of the positive domain in the T3-treated condition. This result was reinforced by mRNA expression analysis of SC markers. Indeed, *Lgr5*, *Olfm4*, *Hopx* and *mTert* mRNAs displayed a higher level of expression in the T3 *versus* control condition, even if in the case of *mTert* the statistical significance was marginal (Fig. 10B). In addition, TH metabolism and transport (*Dio1*

and *Mct10* mRNA expression) remained unaffected by T3 in animals *in vivo* (Fig. S10). Finally, GFP-positive cells were also analyzed by cytometry, but given the mosaic GFP expression in *Lgr5*-EGFP mice (Barker et al., 2007), the results were highly variable even within the same experimental group. Altogether, our observations in mice suggest a role for T3 in inducing an increase in crypt size and proliferation, as well as an increase in the pool of SCs and of Paneth cells.

## DISCUSSION

Despite increasing data on the effect of altered TH levels or TR $\alpha$ 1 expression on intestinal development and homeostasis in mammals, most of the knowledge gathered so far concerns intestinal progenitors, whereas specific analyses focusing on SC biology are lacking. Conversely, extensive research has been conducted on the T3-dependent role in inducing adult intestinal structuration and SC



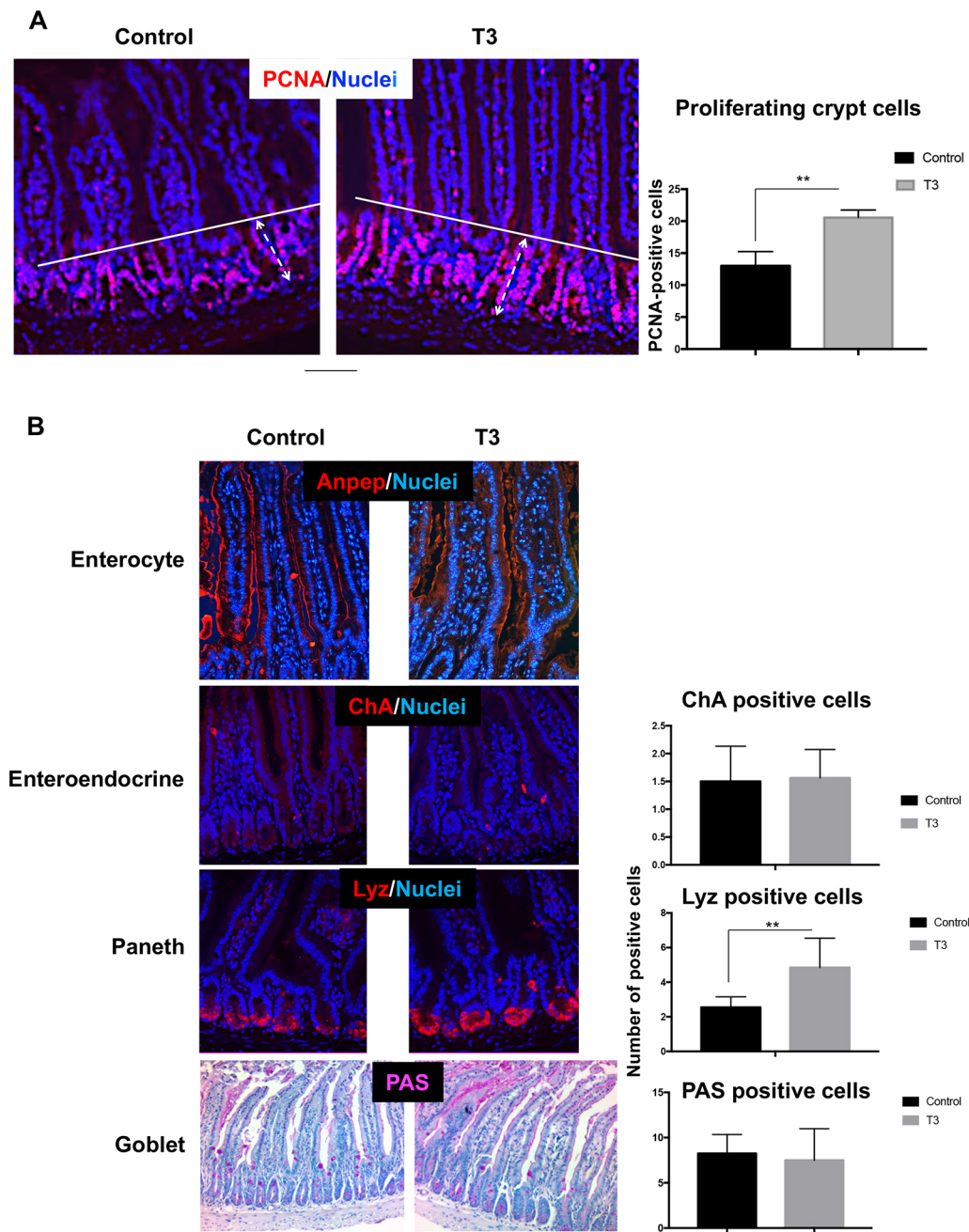


**Fig. 9. Effect of T3 treatment *in vivo*.** (A) Analysis of PCNA-positive proliferating cells in distal small intestinal sections from *Lgr5-EGFP* animals in control or T3 conditions. The images show merged PCNA (red) and nuclear staining (blue). Pictures are representative of three animals per condition. Quantification of PCNA-positive cells scored under a Zeiss imager microscope shown on right. The white line delineates the PCNA-positive crypt compartment; the white dotted double-arrow indicates the crypt length. (B) Analysis of differentiation markers in distal small intestinal sections of control or T3-treated mice as indicated. ANPEP (enterocytes), lysozyme (LYZ, Paneth cells) and chromogranin A (ChA, enteroendocrine cells) were analyzed by immunolabeling. The images show merged differentiation marker (red) and nuclear staining (blue). Mucus-producing goblet cells were stained with PAS. Pictures are representative of three animals per condition. Quantification of positive cells for each differentiation marker scored under a Zeiss imager microscope shown on right. \*\* $P < 0.01$ ,  $n = 30$ . Scale bars: 10  $\mu\text{m}$  (A, B, ANPEP, ChA, Lyz); 20  $\mu\text{m}$  (PAS).

appearance in amphibians during metamorphosis (Frau et al., 2017; Ishizuya-Oka et al., 2009; Shi et al., 2011). Studies in mammals were hindered by a lack of cellular models to examine intestinal SCs. Indeed, discoveries relied exclusively on *in vivo* studies or on 2D primary cultures; these latter, however, presented multiple limitations, including the lack of vertical structuration of the epithelium and of cell hierarchy (Evans et al., 1994). These limitations became obsolete following the establishment of *ex vivo*

3D organoid cultures that represent a powerful tool to study SC self-renewal and multipotency properties (Sato et al., 2009). Thus, studies from the literature and our previous results strongly compelled us to analyze the effect of T3 treatment in intestinal organoids. We decided on the one hand to use a global approach to depict the molecular impact at the transcriptome level of T3 short-term treatment and, on the other hand, to follow the properties of organoid growth and structuration upon addition of T3. Both

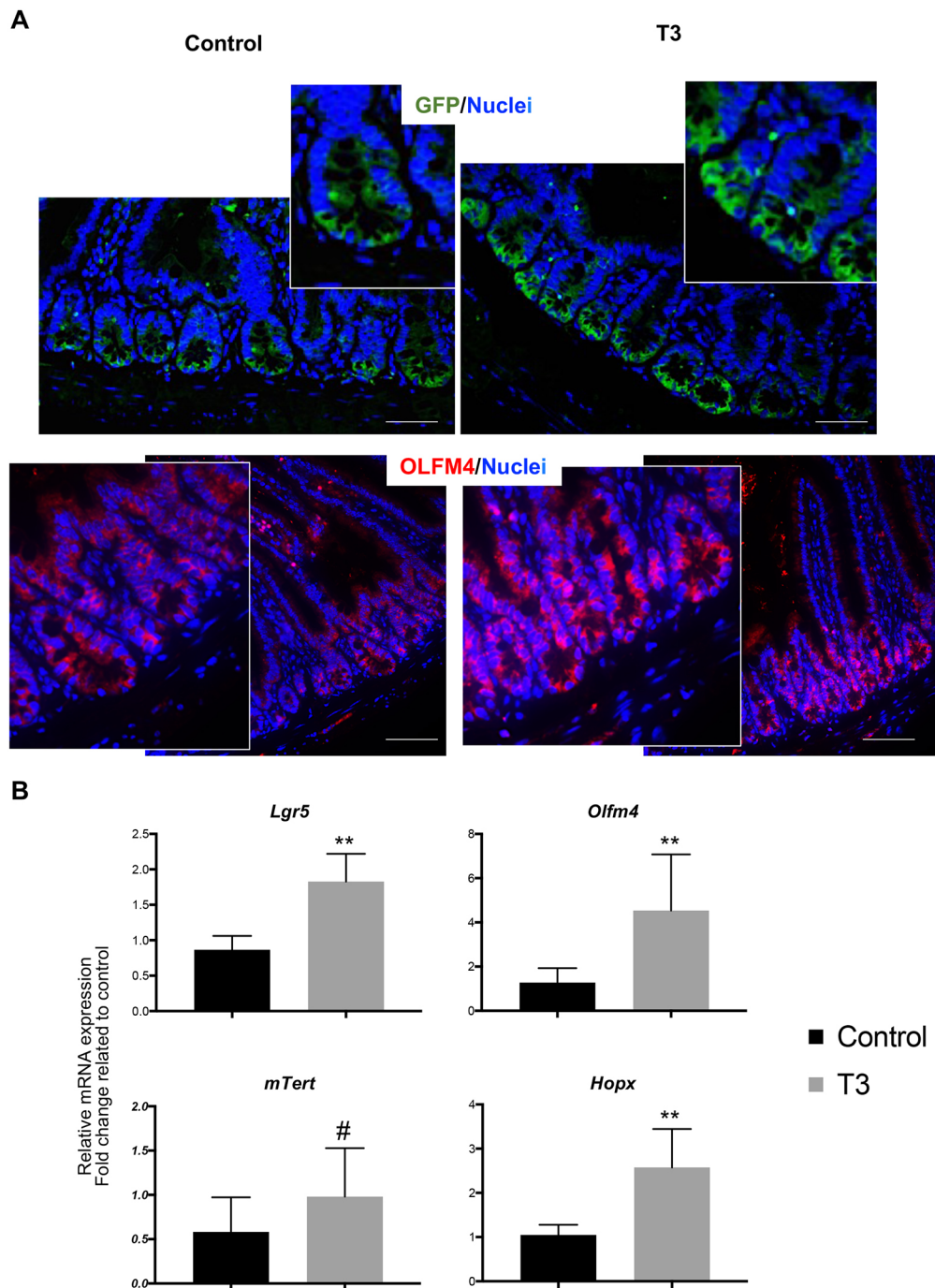


**Fig. 10. Effect of T3 treatment on crypt stem cells *in vivo*.** (A) Stem cells were analyzed in distal small intestinal sections of control or T3-treated mice by immunolabeling for GFP or OLFM4 expression. The images show merged GFP (green) or OLFM4 (red) and nuclear staining (blue). Pictures are representative of three different animals per condition. (B) RT-qPCR analysis of stem cell markers *Lgr5*, *Olfm4*, *Hopx* and *mTert* performed on RNA extracted from the distal small intestinal mucosa. Histograms represent mean  $\pm$  s.d.,  $n=6$ , after normalization against *Ppib*. Data are represented as fold change relative to the control condition. \*\* $P<0.01$ . #, marginal significance ( $P=0.11$ ). Scale bars: 10  $\mu$ m for GFP; 5  $\mu$ m, GFP insets; 15  $\mu$ m for OLFM4; 7.5  $\mu$ m for OLFM4 insets.

approaches were strongly informative and enabled us to define an early and complex response of SCs and progenitors to T3.

Molecular analyses revealed that the first clear-cut response to T3 signaling was at the level of SCs and we named it 'thyroid shock'. Indeed, *Dio1* and *Mct10* mRNA expression were strongly upregulated at each time point analyzed, suggesting a cell defense mechanism in response to high T3 levels (i.e. DIO1 allows T3 degradation and MCT10 transporter regulates its efflux from the cells) (Bianco and da Conceição, 2018; Groeneweg et al., 2017). This response is reminiscent of that observed in the placenta to stop the entry of high TH levels into the bloodstream of embryos or of that of the nervous system during development in the case of hyperthyroidism (Báñez-López and Guadano-Ferraz, 2017; Patel

et al., 2011). Regarding the transcriptome analysis, we observed that among the functions highly represented within the differentially regulated genes (up and down) were stress regulators, transporters and metabolism. For metabolism, in particular, it was evident that enzymes involved in energy metabolism, including glycolysis and lipid metabolism, were largely represented. This high metabolic response is in line with the function of T3 as a metabolic hormone (Cicatiello et al., 2018; Mullur et al., 2014) and with the phenotype observed at an early time point of T3 treatment, illustrated by an accelerated cell turnover. The stress response might be linked with the accelerated turnover and with the SC-associated phenotype. For a thorough comprehension at the level of cell populations, we compared the list of our T3-dependent DEGs with that defining SC

or progenitor gene signatures (Munoz et al., 2012; Sato et al., 2009). We observed that the genes upregulated in the T3 condition were more strongly and significantly associated with the progenitor-like signature than that of SCs. However, upregulated genes belonging to or described as markers of reserve/slow cycling/revival SCs were significantly associated with the SC gene signature. This result, together with the late phenotype of T3-treated organoids (i.e. attenuation of the GFP signal and/or decrease of the GFP-positive cells) strongly indicates that the progressive loss of active *Lgr5*-EGFP SCs might be counterbalanced by the activation and/or the mobilization of other highly plastic crypt cells. These features are commonly observed in animals *in vivo* as a consequence of an injury or of a stress inducing the loss of active SCs (Barker et al., 2010; Beumer and Clevers, 2016; Murata et al., 2020), but are not recapitulated in organoids. Indeed, an intestinal organoid, is a simplified mini-gut composed of the epithelium alone (Date and Sato, 2015) and is not able to overcome the loss of active SCs because the environment (epithelial cell types and culture medium) does not recapitulate all of the signals from the niche (Durand et al., 2012). It is thus not surprising that we observed an increase in reserve SCs markers (*Clu* or *Hopx*), which did not, however, result in an increase or an induction of SCs in response to continuous T3 treatment. Co-culture experiments including organoids and intestinal-derived fibroblasts will be instrumental to shed more light onto the T3-mediated phenotype and the signal exchanged. We expect mechanisms at work to be similar to those described in intestinal tadpole-derived epithelial monocultures or in co-cultured epithelium-mesenchymal tissues, in which T3 can have no/deleterious effects, or act as an inducer of the adult epithelium and the appearance of SCs, respectively (Ishizuya-Oka et al., 2009; Shi et al., 2011).

*Lgr5*-EGFP mice enabled us to specifically track and target the SCs (Barker et al., 2007) both *ex vivo* and *in vivo*. T3 treatment in organoids in the first 2 days induced faster organoid formation and cell proliferation. However, this increased turnover at longer T3 treatment times was responsible for increased cell death and unbalanced cell differentiation, in particular toward goblet cells. Although we did not focus specifically on the biological mechanisms involved, we can speculate that the induction of goblet cells in organoids could arise from altered Notch signaling in the presence of a milder or unaffected Wnt, as suggested by other studies (Gehart and Clevers, 2019; Spit et al., 2018; Yin et al., 2014). T3 treatment *in vivo* increased cell proliferation and also affected cell differentiation potential toward Paneth cells. This result strongly suggests that in animals *in vivo* T3 induces Paneth cell differentiation through an action on Wnt activity (reviewed by Skah et al., 2017). Importantly, Paneth cells constitute and participate in the SC niche, as they provide signals important for SC physiology (Gehart and Clevers, 2019; Spit et al., 2018; Yin et al., 2014). We then hypothesized and experimentally proved that in animals *in vivo* T3 induces an increase in the number of SCs and the expression of SC markers, according to the increased number of 'Paneth/niche cells'.

Taking into account similarities and differences between *in vivo* and *ex vivo* settings, our data underline that T3 acts in an epithelial cell-autonomous manner by inducing an increase in cell proliferation, resulting in an amplification of the progenitor pool in both cases. However, as already commented, SC number and activity are differently affected by T3 when comparing the two systems. Indeed, complex cell interactions, including the presence of specific cell types as well as signals constituting the SC niche, are necessary for SC maintenance and activity (Gehart and Clevers, 2019; Spit et al., 2018; Yin et al., 2014). These signals are lacking or are lost in organoids treated with T3 for longer periods of time.

It is worth noting that the effect of T3 on intestinal epithelial crypt cells and on the self-renewal capacity of organoids (measured by the developmental characteristics and colony forming efficacy) is TR $\alpha$ 1-dependent both *ex vivo* and *in vivo*, as TR $\alpha$ <sup>0/0</sup> organoids have a lower stem cell capacity compared with WT and TR $\beta$ <sup>-/-</sup> organoids. The induction of a dominant negative TR $\alpha$ 1 protein was even more deleterious than complete TR $\alpha$ -gene loss. This is not surprising as constitutive knockout animals very often present an adaptive response to gene loss that can involve newly acquired functions of homologous genes, as previously described for the genes encoding retinoic acid nuclear receptors RAR (Benbrook et al., 2014) or for the Notch genes (Riccio et al., 2008). Redundancy, total or partial, has also been demonstrated in the case of TR $\alpha$  or TR $\beta$  knockout animals in several organs (Contreras-Jurado et al., 2011, 2014; Gullberg et al., 2002; Plateroti et al., 1999). We also observed that T3 treatment or TR $\alpha$ 1 modulation *in vivo* resulted in a very similar intestinal crypt phenotype. Indeed, in addition to the direct correlation between TH or TR $\alpha$ 1 levels and progenitor proliferation, we also observed a correlation with SC number and the expression of SC markers (Fig. 10; Fig. S11). However, TR $\alpha$ 1-modulation gave rise to a stronger phenotype, probably owing to its effects on crypt epithelial cells exclusively, whereas T3 injections can target all the organism and have both direct and indirect effects. Moreover, we cannot completely rule out an involvement of TR $\beta$  in the T3 phenotype when considering that TR $\alpha$ 1 is enriched in precursor cells, whereas TR $\beta$  is enriched in differentiated cells (Sirakov et al., 2014), possibly affecting the expression of genes in the differentiated compartment having, in turn, an effect on SCs.

In conclusion, our data on T3 and TR $\alpha$ 1 on intestinal crypt SCs highlight complex and epithelial cell-autonomous as well as non-autonomous effects. On the one hand, TR $\alpha$ 1 has a primary and direct effect on stem and progenitor cells and it is important for SC maintenance and biology. On the other hand, T3 plays a pleiotropic role that it is more complex to dissect. Indeed, our data underline that 3D organoids are a key model for dissecting early events occurring at the level of SCs, as well as progenitors, in a cell-autonomous manner. However, we should also take into account that the activity of SCs in both organogenesis and homeostasis is niche dependent (Gehart and Clevers, 2019; Spit et al., 2018; Yin et al., 2014). Hence, when studying changes occurring in proliferation, apoptosis and cell differentiation upon biological stimuli such as T3, the organoid system presents important limitations. Such limitations should, however, be overcome by the isolation and study of the various functions of T3 in specific cell populations by using a larger panel of appropriate markers or live-cell reporters. Finally, given that SCs have been clearly identified as the cells of origin of cancers in the intestine (Barker et al., 2009), new advances will help in the development of new tools in the field of precision medicine to target specific cell types, for which T3 has a pro-tumoral impact while preserving the other intestinal epithelial cell types.

## MATERIALS AND METHODS

### Animals and sample collection

We used male and female adult (2- to 4-month-old) *Lgr5*-EGFP-IRES-CreERT2 (*Lgr5*-EGFP) (Barker et al., 2007), TR $\alpha$ <sup>0/0</sup> (Gauthier et al., 2001), TR $\beta$ <sup>-/-</sup> (Gauthier et al., 1999) and TRami (Quignodon et al., 2007). Animals were maintained in a C57BL6/J genetic background. TRami mice were crossed with *Lgr5*-EGFP and *Rosa*-Tomato mice (Madisen et al., 2010) to generate tamoxifen-inducible triple transgenic mice. Animals were housed in the same animal facility and received standard mouse chow and



water *ad libitum*. All experiments were performed in compliance with the French and European guidelines for experimental animal studies and approved by the local committees 'Comités d'Éthique Ceccapp' (C2EA55), the Ministère de l'Enseignement Supérieur et de la Recherche Scientifique, Direction Générale de la Recherche et l'Innovation, Secrétariat 'Autorisation de projet' (agreement #13313-2017020210367606).

For T3 injections, a dose of 20 µg per 20 g body weight in 100 µl saline solution was used; mice were injected once a day for 2 days, controls received 100 µl of saline solution. Mice were sacrificed and intestinal samples were collected in 4% paraformaldehyde (PFA) or liquid nitrogen for paraffin embedding or molecular studies, respectively.

For tamoxifen injections, TRami mice received 100 µl of a 10 mg/ml solution in sunflower oil once a day for 5 days; controls received 100 µl of oil injections. After sacrifice, the intestine was removed for crypt preparation and organoid cultures or collected in 4% PFA or liquid nitrogen for paraffin embedding or molecular studies, respectively.

### Isolation of small intestinal crypts, organoid cultures and treatments

Small intestine (from the proximal jejunum to the distal ileum) was harvested, washed with ice-cold 1× PBS, opened longitudinally to remove luminal content and finally cut into small pieces of 1–2 mm. Pieces of tissue were dynamically washed in ice-cold PBS at 4°C for 20 min. PBS was removed and fragments were incubated in a 2 mM EDTA/PBS solution for 30 min at 4°C. Fragments were then gently mixed with the pipette and the EDTA solution was removed. Intestinal fragments were dynamically washed in PBS and fragments were then shaken to dissociate crypts from the mesenchyme. Supernatant was recovered, giving rise to a crypt-enriched suspension. This suspension was centrifuged at 200 g for 3 min at 4°C and supernatant was removed. The crypt-enriched suspension was filtered through a 70 µm strainer and crypts were slowly centrifuged. Supernatant was removed and organoid culture medium was gently added to the crypt pellet. Finally, Matrigel matrix (Corning) was added to the crypt-medium solution at a 1:1 ratio and drops of 50 µl were then plated in 12-well plates. Finally, 900 µl of organoid culture medium was added to each well. Organoids were cultured at 37°C, 5% CO<sub>2</sub> in IntestiCult Organoid Growth Medium (Stemcell Technologies). Medium was changed every 4 days and organoids replicated approximately every 4/5 days. For replication, Matrigel-embedded organoids were grossly dissociated with a micropipette and fragments were recovered. The equivalent of four dissociated culture-drops were collected in tubes and the volume was adjusted to 5 ml with DMEM. Finally, organoids were mixed, centrifuged and pellets resuspended in IntestiCult/Matrigel mix (1:1 volume) and plated in 50 µl drops, covered by 900 µl of culture medium in 12-well plates.

Organoid development studies over several days in culture were performed on freshly isolated crypt cultures. Live microscopy (bright-field or UV light) and counting of the different structures was carried out using a Zeiss AxioVert inverted microscope. For treatment experiments, T3 was used at a final concentration of 10<sup>-7</sup> M in the culture medium; the stock solution (100×) was prepared in PBS containing 10% bovine serum albumin (BSA); 3,3'-T2 and tetraiodoacetic acid (Tetrac) were used at 10<sup>-7</sup> M; T4 was used at 10<sup>-6</sup> M (Merck-Sigma).

For proliferation studies, control or T3-treated organoids were incubated with 10 µM EdU solution (Click-it Plus Edu Assay Invitrogen, #C10636) for 2 h. After recovery, they were fixed in 4% PFA for 30 min, washed three times with PBS, for 5 min each, before adding 100 µl of 1× Click-it Plus permeabilization buffer to each sample for 15 min at room temperature. At the end of the permeabilization step, 500 µl of Click-it Plus reaction cocktail was added to each tube and samples were incubated for 30 min at room temperature, protected from light and in mild agitation. During the last 10 min of the reaction, 10 mg/ml of Hoechst was added to obtain a final dilution of 1:1000 in each tube. Finally, organoids were washed three times with PBS and mounted with Mowiol [6 g glycerol, 2.4 g mowiol 4-88, 6 ml H<sub>2</sub>O, 12 ml Tris-Cl 0.2 M (pH 8.5) and 1% DABCO].

Growth analysis was performed at different time points in organoids cultured in 96-well round bottom plates. Metabolically active/living cells were analyzed by the tetrazolium salts reduction method (WST-1, Sigma-Aldrich) following the manufacturer's instructions (20 µl of WST-1 solution

in 200 µl of culture medium from each well). The amount of formazan dye formed, directly correlated with the number of metabolically active cells in the culture, was measured using the CLARIOstar apparatus (BMG LABTech) at 450 nm.

For organoid colony assay experiments, organoids were recovered, incubated in Matrisperse (Corning) to eliminate the Matrigel, then incubated in TripLE express solution (Gibco, Thermo Fisher Scientific) at 37°C for 10 min and finally mechanically dissociated using a 1 ml pipette. Dissociation efficiency was directly monitored under the microscope. Cell suspensions were recovered in PBS, washed and filtered in a 40 µm strainer and 5000 single cells per 50 µl of Matrigel drop were plated onto 12-well plates.

### Genomic DNA extraction and PCR analysis

Genomic DNA was extracted from TRami animals or organoids. CRE-mediated deletion was identified by PCR as described in Quignodon et al. (2007). Primers used were: b, 5'-GCCTTCTATCGCCTTCTTGACG; d, 5'-TCCACAGGTATCTCCAGACAGG; e, 5'-GATTCTTCTGGATTGTGCGGCG.

### RNA extraction and RTqPCR

Total RNA was extracted using the Nucleospin RNA Kit (Macherey-Nagel, Fisher Scientific). To remove contaminating genomic DNA (gDNA), DNase digestion was performed on all preparations. Reverse transcription (RT) was performed with the iScript reverse transcriptase (Bio-Rad) on total RNA according to the manufacturer's instructions. To further exclude gDNA contamination after RT we conducted a PCR in all preparations to amplify a housekeeping gene (*Hprt*) for which the primers are located on different exons of the corresponding gene. For qPCR approaches the SYBR qPCR Premix Ex Taq II (Tli RNaseH Plus, Takara) was used in a CFX connect apparatus (Bio-Rad). In each sample, specific mRNA expression was quantified using the ΔCt method and values normalized against *Ppib* levels. Primers are listed in Table S6.

### Protein extraction and western blotting

Protein samples from organoids (50 µg per lane) were prepared with RIPA buffer as described in Uchuya-Castillo et al. (2018), separated by SDS-PAGE and transferred to PVDF membranes 0.2 µm (Bio-Rad). Membranes were blocked with TBS-Tween (Euromedex) supplemented with 5% non-fat milk before incubation with primary antibodies. This step was followed by incubation with HRP-conjugated secondary antibodies (Promega). The signal was analyzed using an enzymatic Clarity substrate detection kit (Bio-Rad) and image detection was performed using a Chemidoc XRS+ imaging system (Bio-Rad), according to manufacturer's protocol. All images were processed using the Image Lab software (Bio-Rad). Antibodies are listed in Table S7.

### RNA-seq analysis

#### Sample preparation for sequencing

Triplicates of organoids maintained in control conditions or treated with 10<sup>-7</sup> M T3 were prepared and processed by Active Motif RNA-seq service (www.activemotif.com). Steps included: isolation of total RNA; assessment of RNA quality/integrity using an Agilent Bioanalyzer; directional library generation and quality control of NGS library; next-generation sequencing using the Illumina platform (GEO accession number: GSE150697).

### Sequencing and analyses

1. Read mapping – standard RNA-seq generates 42-nt sequence reads using Illumina NextSeq 500. The reads were mapped to the genome using the STAR algorithm with default settings (Dobin et al., 2013). Alignment information for each read is stored in the BAM format.
2. Fragment assignment – this process step is to count the number of reads (for single-end library) or fragments (for paired-end library) overlapping predefined genomic features of interest (e.g. genes). Only read pairs that had both ends aligned were counted. Read pairs that had their two ends mapping to different chromosomes or mapping to

the same chromosome but on different strands were discarded. We also required at least 25 bp overlapping bases in a fragment for read assignment. The gene annotations we used were obtained from Subread package (Liao et al., 2014). These annotations were originally from NCBI RefSeq database and then adapted by merging overlapping exons from the same gene to form a set of disjoint exons for each gene. Genes with the same Entrez gene identifiers were also merged into one gene (Liao et al., 2014).

- Differential analysis – after obtaining the gene table containing the fragment (or read) counts of genes, differential analysis was performed to identify statistically significant differential genes using DESeq2 (Love et al., 2014). The following two pre-processing steps were used before differential calling. (1) Data normalization: DESeq2 expects an un-normalized count matrix of sequencing reads (for single-end RNA-seq) or fragments (for paired-end RNA-seq) for the DESeq2 statistical model to hold. The DESeq2 model internally corrects for library size using the median-of-ratios method (Love et al., 2014). The gene table obtained from fragment assignment was used as input to perform the DESeq2 differential test. (2) Filtering before multiple testing adjustment: after a differential test has been applied to each gene except the ones with zero counts, the *P*-value of each gene was calculated and needed to be further adjusted to control the number of false positives among all discoveries at a proper level. This procedure is known as multiple testing adjustment. During this process, DESeq2 by default filters out statistical tests (i.e. genes) that have low counts by a statistical technique called independent filtering. It uses the average counts of each gene (i.e. baseMean), across all samples, as its filter criterion, and it omits all genes with average normalized counts below a filtering threshold from multiple testing adjustment. This filtering threshold was automatically determined to maximize detection power (i.e. maximize the number of differential genes detected) at a specified false discovery rate (FDR).
- Filtering criteria – DEGs were filters for  $\text{shrunkenLog2FC} > 0.5$  and adjusted *P*-value 0.05. The adjusted *P*-value was generated by Benjamini and Hochberg's FDR procedure and it is commonly used to evaluate statistical significance after multiple testing adjustment.

### GO and pathway enrichment analysis

To classify the functions of DEGs, GO enrichment and Reactome pathway (Fabregat et al., 2016) analysis were performed using Panther (Mi et al., 2005) or Ingenuity Pathway Analysis (Ingenuity® Systems, www.ingenuity.com). For both analyses we considered terms to be significant if the FDR adjusted *P*-values were  $< 0.05$  and fold enrichment was  $> 2.0$ . Furthermore, we used REVIGO (Supek et al., 2011) to reduce redundancy of the enriched GO terms and visualize the semantic clustering of the identified top scoring terms. GSEA was performed using Enricher (Kuleshov et al., 2016) and with fast Gene Set Enrichment Analysis Package (version 1.9.7) implemented in R software. This analysis compared genes differentially expressed between T3-treated and control organoids and the Lgr5-GFP<sup>High</sup> intestinal stem cell signature or Lgr5-GFP<sup>Low</sup> progenitor signature as described previously (Munoz et al., 2012). Our dataset was compared with two studies (GSE23672 – stem cells versus progenitor cells; GSE25109 – stem cells versus Paneth cells) and to the stem cell gene signature defined by Munoz et al. (2012).

### Gene interaction network analysis

In order to determine the association between genes in a given dataset, a protein-protein interaction network was constructed using the STRING database (v10) (Szklarczyk et al., 2015). The interactions were based on experimental evidence, co-occurrence and text-mining.

### Immunofluorescence, histological staining and microscopy

For *in vivo* experiments, formalin-fixed paraffin-embedded (FFPE) sections (5  $\mu\text{m}$  thickness) were used for indirect immunostaining. Briefly, the sections were processed to eliminate paraffin and then incubated with primary antibodies overnight at 4°C followed by incubation with fluorescent secondary antibodies (Alexa Fluor, Molecular Probes, 1:1000). All nuclei were counterstained with Hoechst (33342, Molecular Probes).

For *ex vivo* experiments, organoids were recovered and fixed in 3% PFA for 15 min at room temperature. They were then incubated in PBS/Triton 0.5% for 30 min, PBS/Triton 0.2%/BSA 1% for 30 min at room temperature. The solution was then discarded and primary antibodies were added at 4°C overnight. Organoids were rinsed in PBS and secondary antibodies were added for 4 h at room temperature. All nuclei were counterstained with Hoechst (33342, Molecular Probes) for 20 min. Finally, organoids were rinsed and mounted on glass slides. Antibodies are listed in Table S7. To label mucus-producing goblet cells, the paraffin sections were subjected to periodic acid-Schiff (PAS) staining as previously reported (Plateroti et al., 1999). Mucin-filled cells were stained in bright fuchsia.

Conventional bright-field and fluorescence microscopy was performed on a Right Zeiss AxioImager 2. All of the pictures were reproducibly modified using the ImageJ software (brightness/contrasts).

### Statistical analysis

Results illustrated as histograms or line graphs represent the mean  $\pm$  s.d. Comparisons between groups were performed using a two-tailed unpaired Student's *t*-test;  $P < 0.05$  was considered to be statistically significant.

### Acknowledgements

We are grateful to Manon Pratviel for her assistance with animal handling and care within the AniCan animal facility (Centre de Recherche en Cancérologie de Lyon; CRCL). We also acknowledge the imaging, cytometry and Anapath recherche small animal histology platforms (CRCL, Centre Léon Bérard). We are indebted to Anne Wierinckx and Joel Lachuer (ProfilExpert platform) for help with the bioinformatics analysis. Special thanks to Drs Elio Biffali and Pasquale De Luca as well as the Sequencing and Molecular Analyses Center personnel for their help in automated plate assembly and Real Time PCR runs at the Stazione Zoologica. We also thank Brigitte Manship for critical reading of the manuscript.

### Competing interests

The authors declare no competing or financial interests.

### Author contributions

Conceptualization: M.G., C.F., J.-N.F., L.O.P., M.S., M.P.; Methodology: M.G., C.F., M.V.G., C.J., C.L.N., M.S., M.P.; Validation: M.G., J.-N.F., M.S., M.P.; Formal analysis: L.O.P.; Investigation: M.G., C.F., D.F., M.V.G., C.J., C.L.N., L.O.P., M.S., M.P.; Resources: C.J., C.L.N.; Data curation: D.F., M.P.; Writing - original draft: M.G., C.F., J.-N.F., L.O.P., M.S., M.P.; Writing - review & editing: M.G., D.F., M.V.G., J.-N.F., L.O.P., M.S., M.P.; Visualization: D.F., M.V.G., M.P.; Supervision: M.P.; Funding acquisition: M.P.

### Funding

The work was supported by the Département du Rhône de la Ligue Contre le Cancer (grant 172190), by the Fondation ARC pour la Recherche sur le Cancer (ARC) (grant PGA1201402000834), by the Fondation pour la Recherche Médicale (FRM) (Equipes FRM 2018, DEQ20181039598) and by the Institut National Du Cancer (PLBIO19-289). M.G. and M.V.G. received support from the FRM; C.F. received support from ARC and the Centre Léon Bérard.

### Data availability

RNA-seq data have been deposited in GEO under accession number GSE150697.

### References

- Amma, L. L., Campos-Barros, A., Wang, Z., Vennström, B. and Forrest, D. (2001). Distinct tissue-specific roles for thyroid hormone receptors  $\beta$  and  $\alpha 1$  in regulation of type 1 deiodinase expression. *Mol. Endocrinol.* **15**, 467-475. doi:10.1210/mend.15.3.0605
- Ayyaz, A., Kumar, S., Sangiorgi, B., Ghoshal, B., Gosio, J., Ouladan, S., Fink, M., Barutcu, S., Trcka, D., Shen, J. et al. (2019). Single-cell transcriptomes of the regenerating intestine reveal a revival stem cell. *Nature* **569**, 121-125. doi:10.1038/s41586-019-1154-y
- Bao, L., Roediger, J., Park, S., Fu, L., Shi, B., Cheng, S.-Y. and Shi, Y.-B. (2019). Thyroid hormone receptor alpha mutations lead to epithelial defects in the adult intestine in a mouse model of resistance to thyroid hormone. *Thyroid* **29**, 439-448. doi:10.1089/thy.2018.0340
- Bárez-López, S. and Guadano-Ferraz, A. (2017). Thyroid hormone availability and action during brain development in rodents. *Front Cell Neurosci* **11**, 240. doi:10.3389/fncel.2017.00240
- Barker, N. (2014). Adult intestinal stem cells: critical drivers of epithelial homeostasis and regeneration. *Nat. Rev. Mol. Cell Biol.* **15**, 19-33. doi:10.1038/nrm3721

- Barker, N., van Es, J. H., Kuipers, J., Kujala, P., van den Born, M., Cozijnsen, M., Haegebarth, A., Korving, J., Begthel, H., Peters, P. J. et al.** (2007). Identification of stem cells in small intestine and colon by marker gene Lgr5. *Nature* **449**, 1003-1007. doi:10.1038/nature06196
- Barker, N., Ridgway, R. A., van Es, J. H., van de Wetering, M., Begthel, H., van den Born, M., Danenberg, E., Clarke, A. R., Sansom, O. J. and Clevers, H.** (2009). Crypt stem cells as the cells-of-origin of intestinal cancer. *Nature* **457**, 608-611. doi:10.1038/nature07602
- Barker, N., Bartfeld, S. and Clevers, H.** (2010). Tissue-resident adult stem cell populations of rapidly self-renewing organs. *Cell Stem Cell* **7**, 656-670. doi:10.1016/j.stem.2010.11.016
- Benbrook, D. M., Chambon, P., Rochette-Egly, C. and Asson-Batres, M. A.** (2014). History of retinoic acid receptors. *Subcell. Biochem.* **70**, 1-20. doi:10.1007/978-94-017-9050-5\_1
- Beumer, J. and Clevers, H.** (2016). Regulation and plasticity of intestinal stem cells during homeostasis and regeneration. *Development* **143**, 3639-3649. doi:10.1242/dev.133132
- Bianco, A. C. and da Conceição, R. R.** (2018). The Deiodinase Trio and Thyroid Hormone Signaling. *Methods Mol. Biol.* **1801**, 67-83. doi:10.1007/978-1-4939-7902-8\_8
- Brent, G. A.** (2012). Mechanisms of thyroid hormone action. *J. Clin. Invest.* **122**, 3035-3043. doi:10.1172/JCI60047
- Chen, G., Korfhagen, T. R., Xu, Y., Kitzmiller, J., Wert, S. E., Maeda, Y., Gregorieff, A., Clevers, H. and Whitsett, J. A.** (2009). SPDEF is required for mouse pulmonary goblet cell differentiation and regulates a network of genes associated with mucus production. *J. Clin. Invest.* **119**, 2914-2924. doi:10.1172/JCI39731
- Cicatiello, A. G., Di Girolamo, D. and Dentice, M.** (2018). Metabolic effects of the intracellular regulation of thyroid hormone: old players, new concepts. *Front. Endocrinol.* **9**, 474. doi:10.3389/fendo.2018.00474
- Contreras-Jurado, C., García-Serrano, L., Gómez-Ferrería, M., Costa, C., Paramio, J. M. and Aranda, A.** (2011). The thyroid hormone receptors as modulators of skin proliferation and inflammation. *J. Biol. Chem.* **286**, 24079-24088. doi:10.1074/jbc.M111.218487
- Contreras-Jurado, C., García-Serrano, L., Martínez-Fernández, M., Ruiz-Lorente, L., Paramio, J. M. and Aranda, A.** (2014). Impaired hair growth and wound healing in mice lacking thyroid hormone receptors. *PLoS ONE* **9**, e108137. doi:10.1371/journal.pone.0108137
- Danopoulos, S., Schlieve, C. R., Grikscheit, T. C. and Al Alam, D.** (2017). Fibroblast growth factors in the gastrointestinal tract: twists and turns. *Dev. Dyn.* **246**, 344-352. doi:10.1002/dvdy.24491
- Date, S. and Sato, T.** (2015). Mini-gut organoids: reconstitution of the stem cell niche. *Annu. Rev. Cell Dev. Biol.* **31**, 269-289. doi:10.1146/annurev-cellbio-100814-125218
- Davis, P. J., Davis, F. B., Mousa, S. A., Luidens, M. K. and Lin, H.-Y.** (2011). Membrane receptor for thyroid hormone: physiologic and pharmacologic implications. *Annu. Rev. Pharmacol. Toxicol.* **51**, 99-115. doi:10.1146/annurev-pharmtox-010510-100512
- Denver, R. J. and Williamson, K. E.** (2009). Identification of a thyroid hormone response element in the mouse Krüppel-like factor 9 gene to explain its postnatal expression in the brain. *Endocrinology* **150**, 3935-3943. doi:10.1210/en.2009-0050
- Dobin, A., Davis, C. A., Schlesinger, F., Drenkow, J., Zaleski, C., Jha, S., Batut, P., Chaisson, M. and Gingeras, T. R.** (2013). STAR: ultrafast universal RNA-seq aligner. *Bioinformatics* **29**, 15-21. doi:10.1093/bioinformatics/bts635
- Durand, A., Donahue, B., Peignon, G., Letourneur, F., Cagnard, N., Slomianny, C., Perret, C., Shroyer, N. F. and Remagnolo, B.** (2012). Functional intestinal stem cells after Paneth cell ablation induced by the loss of transcription factor Math1 (Atoh1). *Proc. Natl. Acad. Sci. USA* **109**, 8965-8970. doi:10.1073/pnas.1201652109
- Evans, G. S., Flint, N. and Potten, C. S.** (1994). Primary cultures for studies of cell regulation and physiology in intestinal epithelium. *Annu. Rev. Physiol.* **56**, 399-417. doi:10.1146/annurev.ph.56.030194.002151
- Fabregat, A., Sidiropoulos, K., Garapati, P., Gillespie, M., Hausmann, K., Haw, R., Jassal, B., Jupe, S., Korninger, F., McKay, S. et al.** (2016). The Reactome pathway Knowledgebase. *Nucleic Acids Res.* **44**, D481-D487. doi:10.1093/nar/gkv1351
- Frau, C., Godart, M. and Plateroti, M.** (2017). Thyroid hormone regulation of intestinal epithelial stem cell biology. *Mol. Cell. Endocrinol.* **459**, 90-97. doi:10.1016/j.mce.2017.03.002
- Gauthier, K., Chassande, O., Plateroti, M., Roux, J. P., Legrand, C., Pain, B., Rousset, B., Weiss, R., Trouillas, J. and Samarut, J.** (1999). Different functions for the thyroid hormone receptors TR $\alpha$  and TR $\beta$  in the control of thyroid hormone production and post-natal development. *EMBO J.* **18**, 623-631. doi:10.1093/emboj/18.3.623
- Gauthier, K., Plateroti, M., Harvey, C. B., Williams, G. R., Weiss, R. E., Refetoff, S., Willott, J. F., Sundin, V., Roux, J.-P., Malaval, L. et al.** (2001). Genetic analysis reveals different functions for the products of the thyroid hormone receptor  $\alpha$  locus. *Mol. Cell. Biol.* **21**, 4748-4760. doi:10.1128/MCB.21.14.4748-4760.2001
- Gehart, H. and Clevers, H.** (2019). Tales from the crypt: new insights into intestinal stem cells. *Nat. Rev. Gastroenterol. Hepatol.* **16**, 19-34. doi:10.1038/s41575-018-0081-y
- Groeneweg, S., Visser, W. E. and Visser, T. J.** (2017). Disorder of thyroid hormone transport into the tissues. *Best Pract. Res. Clin. Endocrinol. Metab.* **31**, 241-253. doi:10.1016/j.beem.2017.05.001
- Gullberg, H., Rudling, M., Saltó, C., Forrest, D., Angelin, B. and Vennström, B.** (2002). Requirement for thyroid hormone receptor  $\beta$  in T3 regulation of cholesterol metabolism in mice. *Mol. Endocrinol.* **16**, 1767-1777. doi:10.1210/me.2002-0009
- Hammes, S. R. and Davis, P. J.** (2015). Overlapping nongenomic and genomic actions of thyroid hormone and steroids. *Best Practice Res. Clin. Endocrinol. Metab.* **29**, 581-593. doi:10.1016/j.beem.2015.04.001
- Ishizuya-Oka, A., Hasebe, T., Buchholz, D. R., Kajita, M., Fu, L. and Shi, Y. B.** (2009). Origin of the adult intestinal stem cells induced by thyroid hormone in *Xenopus laevis*. *FASEB J.* **23**, 2568-2575. doi:10.1096/fj.08-128124
- Kalyanaraman, H., Schwappacher, R., Joshua, J., Zhuang, S., Scott, B. T., Klos, M., Casteel, D. E., Frangos, J. A., Dillmann, W., Boss, G. R. et al.** (2014). Nongenomic thyroid hormone signaling occurs through a plasma membrane-localized receptor. *Sci. Signal.* **7**, ra48. doi:10.1126/scisignal.2004911
- Kim, J.-Y., Jeong, H. S., Chung, T., Kim, M., Lee, J. H., Jung, W. H. and Koo, J. S.** (2017). The value of phosphohistone H3 as a proliferation marker for evaluating invasive breast cancers: a comparative study with Ki67. *Oncotarget* **8**, 65064-65076. doi:10.18632/oncotarget.17775
- Kress, E., Rezza, A., Nadjar, J., Samarut, J. and Plateroti, M.** (2009). The frizzled-related sFRP2 gene is a target of thyroid hormone receptor  $\alpha$ 1 and activates  $\beta$ -catenin signaling in mouse intestine. *J. Biol. Chem.* **284**, 1234-1241. doi:10.1074/jbc.M806548200
- Kress, E., Skah, S., Sirakov, M., Nadjar, J., Gadot, N., Scozecz, J. Y., Samarut, J. and Plateroti, M.** (2010). Cooperation between the thyroid hormone receptor TR $\alpha$ 1 and the WNT pathway in the induction of intestinal tumorigenesis. *Gastroenterology* **138**, 1863-1874.e1. doi:10.1053/j.gastro.2010.01.041
- Kuleshov, M. V., Jones, M. R., Rouillard, A. D., Fernandez, N. F., Duan, Q., Wang, Z., Koplev, S., Jenkins, S. L., Jagodnik, K. M., Lachmann, A. et al.** (2016). Enrichr: a comprehensive gene set enrichment analysis web server 2016 update. *Nucleic Acids Res.* **44**, W90-W97. doi:10.1093/nar/gkw377
- Li, L. and Clevers, H.** (2010). Coexistence of quiescent and active adult stem cells in mammals. *Science* **327**, 542-545. doi:10.1126/science.1180794
- Liao, Y., Smyth, G. K. and Shi, W.** (2014). featureCounts: an efficient general purpose program for assigning sequence reads to genomic features. *Bioinformatics* **30**, 923-930. doi:10.1093/bioinformatics/btt656
- Love, M. I., Huber, W. and Anders, S.** (2014). Moderated estimation of fold change and dispersion for RNA-seq data with DESeq2. *Genome Biol.* **15**, 550. doi:10.1186/s13059-014-0550-8
- Madisen, L., Zwingman, T. A., Sunkin, S. M., Oh, S. W., Zariwala, H. A., Gu, H., Ng, L. L., Palminter, R. D., Hawrylycz, M. J., Jones, A. R. et al.** (2010). A robust and high-throughput Cre reporting and characterization system for the whole mouse brain. *Nat. Neurosci.* **13**, 133-140. doi:10.1038/nn.2467
- Mi, H., Lazareva-Ulitsky, B., Loo, R., Kejarival, A., Vandergriff, J., Rabkin, S., Guo, N., Muruganujan, A., Doremieux, O., Campbell, M. J., Kitano, H. and Thomas, P. D.** (2005). The PANTHER database of protein families, subfamilies, functions and pathways. *Nucleic Acids Res.* **33**, D284-D288. doi:10.1093/nar/gki078
- Mullur, R., Liu, Y.-Y. and Brent, G. A.** (2014). Thyroid hormone regulation of metabolism. *Physiol. Rev.* **94**, 355-382. doi:10.1152/physrev.00030.2013
- Munoz, J., Stange, D. E., Schepers, A. G., van de Wetering, M., Koo, B.-K., Itzkovitz, S., Volckmann, R., Kung, K. S., Koster, J., Radulescu, S. et al.** (2012). The Lgr5 intestinal stem cell signature: robust expression of proposed quiescent '4' cell markers. *EMBO J.* **31**, 3079-3091. doi:10.1038/emboj.2012.166
- Murata, K., Jadhav, U., Madha, S., van Es, J., Dean, J., Cavazza, A., Wucherpfennig, K., Michor, F., Clevers, H. and Ramesh, A. et al.** (2020). Ascl2-dependent cell dedifferentiation drives regeneration of ablated intestinal stem cells. *Cell Stem Cell* **26**, 377-390.e6. doi:10.1016/j.stem.2019.12.011
- Nielsen, P. S., Riber-Hansen, R., Jensen, T. O., Schmidt, H. and Steiniche, T.** (2013). Proliferation indices of phosphohistone H3 and Ki67: strong prognostic markers in a consecutive cohort with stage I/II melanoma. *Mod. Pathol.* **26**, 404-413. doi:10.1038/modpathol.2012.188
- Noah, T. K., Donahue, B. and Shroyer, N. F.** (2011). Intestinal development and differentiation. *Exp. Cell Res.* **317**, 2702-2710. doi:10.1016/j.yexcr.2011.09.006
- Patel, J., Landers, K., Li, H., Mortimer, R. H. and Richard, K.** (2011). Delivery of maternal thyroid hormones to the fetus. *Trends Endocrinol. Metab.* **22**, 164-170. doi:10.1016/j.tem.2011.02.002
- Plateroti, M., Chassande, O., Fraichard, A., Gauthier, K., Freund, J. N., Samarut, J. and Keding, M.** (1999). Involvement of T3R $\alpha$ - and  $\beta$ -receptor subtypes in mediation of T3 functions during postnatal murine intestinal development. *Gastroenterology* **116**, 1367-1378. doi:10.1016/S0016-5085(99)70501-9
- Plateroti, M., Gauthier, K., Domon-Delli, C., Freund, J.-N., Samarut, J. and Chassande, O.** (2001). Functional interference between thyroid hormone receptor  $\alpha$  (TR $\alpha$ ) and natural truncated TR $\alpha$  isoforms in the control of intestine



- development. *Mol. Cell. Biol.* **21**, 4761-4772. doi:10.1128/MCB.21.14.4761-4772.2001
- Plateroti, M., Kress, E., Mori, J. I. and Samarut, J.** (2006). Thyroid hormone receptor  $\alpha 1$  directly controls transcription of the  $\beta$ -catenin gene in intestinal epithelial cells. *Mol. Cell. Biol.* **26**, 3204-3214. doi:10.1128/MCB.26.8.3204-3214.2006
- Quignodon, L., Vincent, S., Winter, H., Samarut, J. and Flamant, F.** (2007). A point mutation in the activation function 2 domain of thyroid hormone receptor  $\alpha 1$  expressed after CRE-mediated recombination partially recapitulates hypothyroidism. *Mol. Endocrinol.* **21**, 2350-2360. doi:10.1210/me.2007-0176
- Riccio, O., van Gijn, M. E., Bezdek, A. C., Pellegrinet, L., van Es, J. H., Zimmer-Strobl, U., Strobl, L. J., Honjo, T., Clevers, H. and Radtke, F.** (2008). Loss of intestinal crypt progenitor cells owing to inactivation of both Notch1 and Notch2 is accompanied by derepression of CDK inhibitors p27Kip1 and p57Kip2. *EMBO Rep.* **9**, 377-383. doi:10.1038/embor.2008.7
- Sato, T., Vries, R. G., Snippert, H. J., van de Wetering, M., Barker, N., Stange, D. E., van Es, J. H., Abo, A., Kujala, P., Peters, P. J. et al.** (2009). Single Lgr5 stem cells build crypt-villus structures in vitro without a mesenchymal niche. *Nature* **459**, 262-265. doi:10.1038/nature07935
- Shi, Y.-B., Hasebe, T., Fu, L., Fujimoto, K. and Ishizuya-Oka, A.** (2011). The development of the adult intestinal stem cells: Insights from studies on thyroid hormone-dependent amphibian metamorphosis. *Cell Biosci* **1**, 30. doi:10.1186/2045-3701-1-30
- Siebel, C. and Lendahl, U.** (2017). Notch signaling in development, tissue homeostasis, and disease. *Physiol. Rev.* **97**, 1235-1294. doi:10.1152/physrev.00005.2017
- Sirakov, M. and Plateroti, M.** (2011). The thyroid hormones and their nuclear receptors in the gut: from developmental biology to cancer. *Biochim. Biophys. Acta* **1812**, 938-946. doi:10.1016/j.bbadis.2010.12.020
- Sirakov, M., Kress, E., Nadjar, J. and Plateroti, M.** (2014). Thyroid hormones and their nuclear receptors: new players in intestinal epithelium stem cell biology? *Cell. Mol. Life Sci.* **71**, 2897-2907. doi:10.1007/s00018-014-1586-3
- Sirakov, M., Boussouar, A., Kress, E., Frau, C., Lone, I. N., Nadjar, J., Angelov, D. and Plateroti, M.** (2015). The thyroid hormone nuclear receptor TR $\alpha 1$  controls the Notch signaling pathway and cell fate in murine intestine. *Development* **142**, 2764-2774. doi:10.1242/dev.121962
- Skah, S., Uchuya-Castillo, J., Sirakov, M. and Plateroti, M.** (2017). The thyroid hormone nuclear receptors and the Wnt/ $\beta$ -catenin pathway: an intriguing liaison. *Dev. Biol.* **422**, 71-82. doi:10.1016/j.ydbio.2017.01.003
- Spit, M., Koo, B. K. and Maurice, M. M.** (2018). Tales from the crypt: intestinal niche signals in tissue renewal, plasticity and cancer. *Open Biol.* **8**, 180120. doi:10.1098/rsob.180120
- Supek, F., Bošnjak, M., Škunca, N. and Šmuc, T.** (2011). REVIGO summarizes and visualizes long lists of gene ontology terms. *PLoS ONE* **6**, e21800. doi:10.1371/journal.pone.0021800
- Szklarczyk, D., Franceschini, A., Wyder, S., Forslund, K., Heller, D., Huerta-Cepas, J., Simonovic, M., Roth, A., Santos, A., Tsafou, K. P. et al.** (2015). STRING v10: protein-protein interaction networks, integrated over the tree of life. *Nucleic Acids Res.* **43**, D447-D452. doi:10.1093/nar/gku1003
- Tian, H., Biehs, B., Chiu, C., Siebel, C. W., Wu, Y., Costa, M., de Sauvage, F. J. and Klein, O. D.** (2015). Opposing activities of Notch and Wnt signaling regulate intestinal stem cells and gut homeostasis. *Cell Rep* **11**, 33-42. doi:10.1016/j.celrep.2015.03.007
- Uchuya-Castillo, J., Aznar, N., Frau, C., Martinez, P., Le Nevé, C., Marisa, L., Penalva, L. O. F., Laurent-Puig, P., Puisieux, A., Scoazec, J.-Y. et al.** (2018). Increased expression of the thyroid hormone nuclear receptor TR $\alpha 1$  characterizes intestinal tumors with high Wnt activity. *Oncotarget* **9**, 30979-30996. doi:10.18632/oncotarget.25741
- Umar, S.** (2010). Intestinal stem cells. *Curr. Gastroenterol. Rep.* **12**, 340-348. doi:10.1007/s11894-010-0130-3
- van der Flier, L. G. and Clevers, H.** (2009). Stem cells, self-renewal, and differentiation in the intestinal epithelium. *Annu. Rev. Physiol.* **71**, 241-260. doi:10.1146/annurev.physiol.010908.163145
- van Es, J. H., van Gijn, M. E., Riccio, O., van den Born, M., Vooijs, M., Begthel, H., Cozijnsen, M., Robine, S., Winton, D. J., Radtke, F. et al.** (2005). Notch/ $\gamma$ -secretase inhibition turns proliferative cells in intestinal crypts and adenomas into goblet cells. *Nature* **435**, 959-963. doi:10.1038/nature03659
- Yin, X., Farin, H. F., van Es, J. H., Clevers, H., Langer, R. and Karp, J. M.** (2014). Niche-independent high-purity cultures of Lgr5<sup>+</sup> intestinal stem cells and their progeny. *Nat. Methods* **11**, 106-112. doi:10.1038/nmeth.2737

## Godart et al, Figure S1

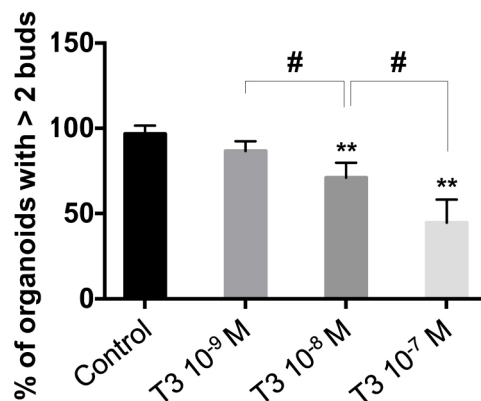


**Figure S1. Test of T3 concentrations on intestinal organoids.** Replicated organoids were maintained in control condition or treated with T3 at different concentrations ( $10^{-7}$  M,  $10^{-8}$  M and  $10^{-9}$  M), as indicated. The percentage of complex organoids ( $> 2$  buds) was analyzed at D4. Histograms represent mean  $\pm$  SD,  $n = 6$ . \*\*,  $P < 0.01$  compared to control; #,  $P < 0.05$  compared to the T3  $10^{-9}$  M condition. This experiment convinced us to choose the  $10^{-7}$  M concentration of T3 for all following experiments.

## Godart et al, Figure S2

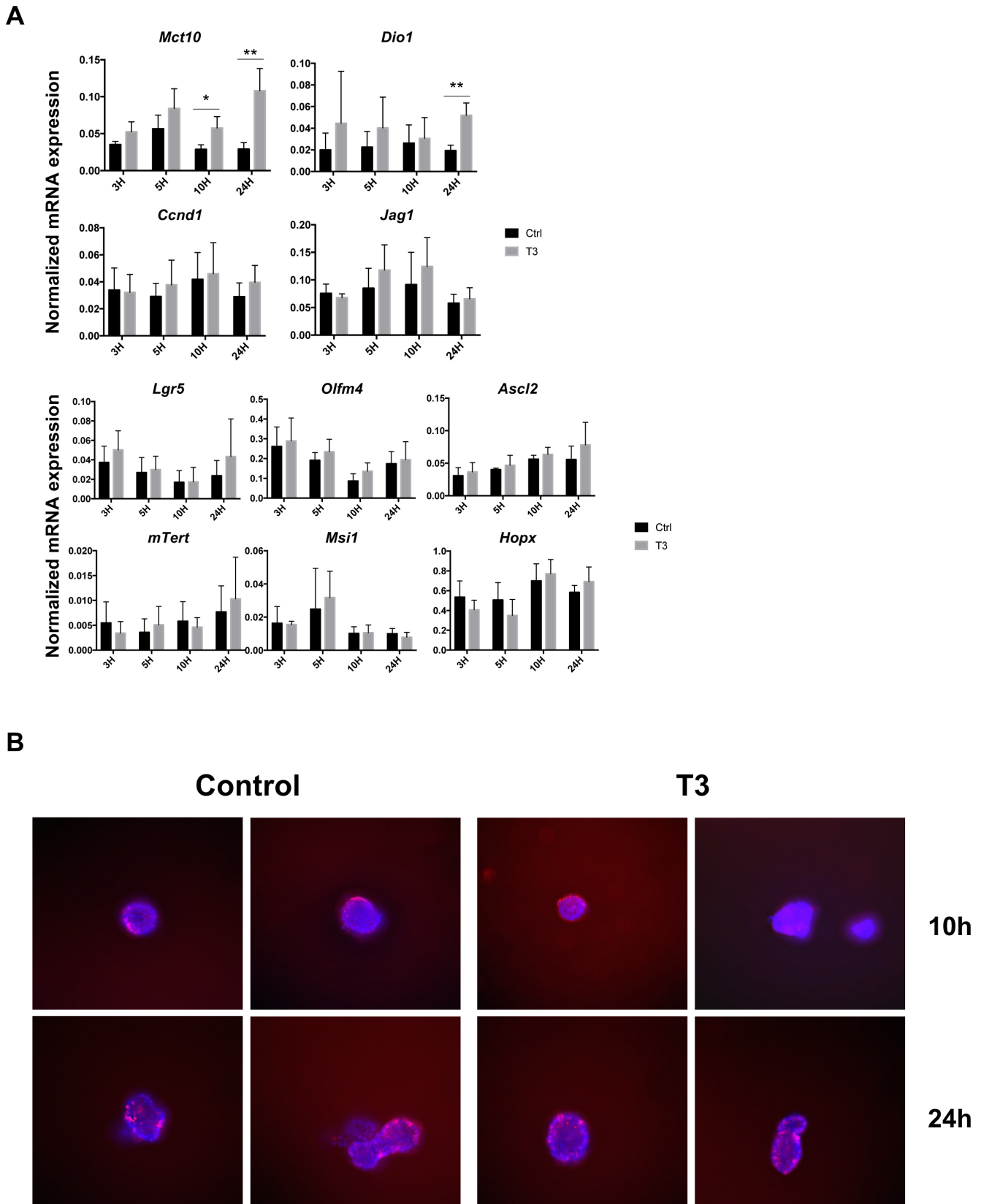




**Figure S2. Short-term treatment of TR $\alpha$ <sup>0/0</sup> organoids with T3.** A) Replicated TR $\alpha$ <sup>0/0</sup> organoids were cultured over 24 h in the absence (Control) or presence of 10<sup>-7</sup> M T3, as indicated. RT-qPCR experiments were performed at different time points, as indicated, to analyze the mRNA expression of the TH metabolizing enzyme *Dio1* and transporter *Mct10*; *Ccnd1* (Cyclin D1) was used as a proliferative marker and *Jag1* as a direct T3-target gene. In addition, stem cell markers *Lgr5*, *Olfm4*, *Ascl2*, *mTert*, *Msi1* and *Hopx* were also analyzed. Histograms represent mean  $\pm$  SD, n = 4, after normalization against *Ppib*. \*,  $P < 0.05$ , \*\*,  $P < 0.01$  compared to the respective control conditions. B) Proliferation analysis by EdU incorporation was performed on organoids in control condition or treated with T3 for 10 h or 24 h; in both cases EdU was added in the culture medium 2 h before ending cultures. Images show merged EdU labeling (red) and nuclear staining (blue). Bar = 7  $\mu$ m.

### Godart et al, Figure S3

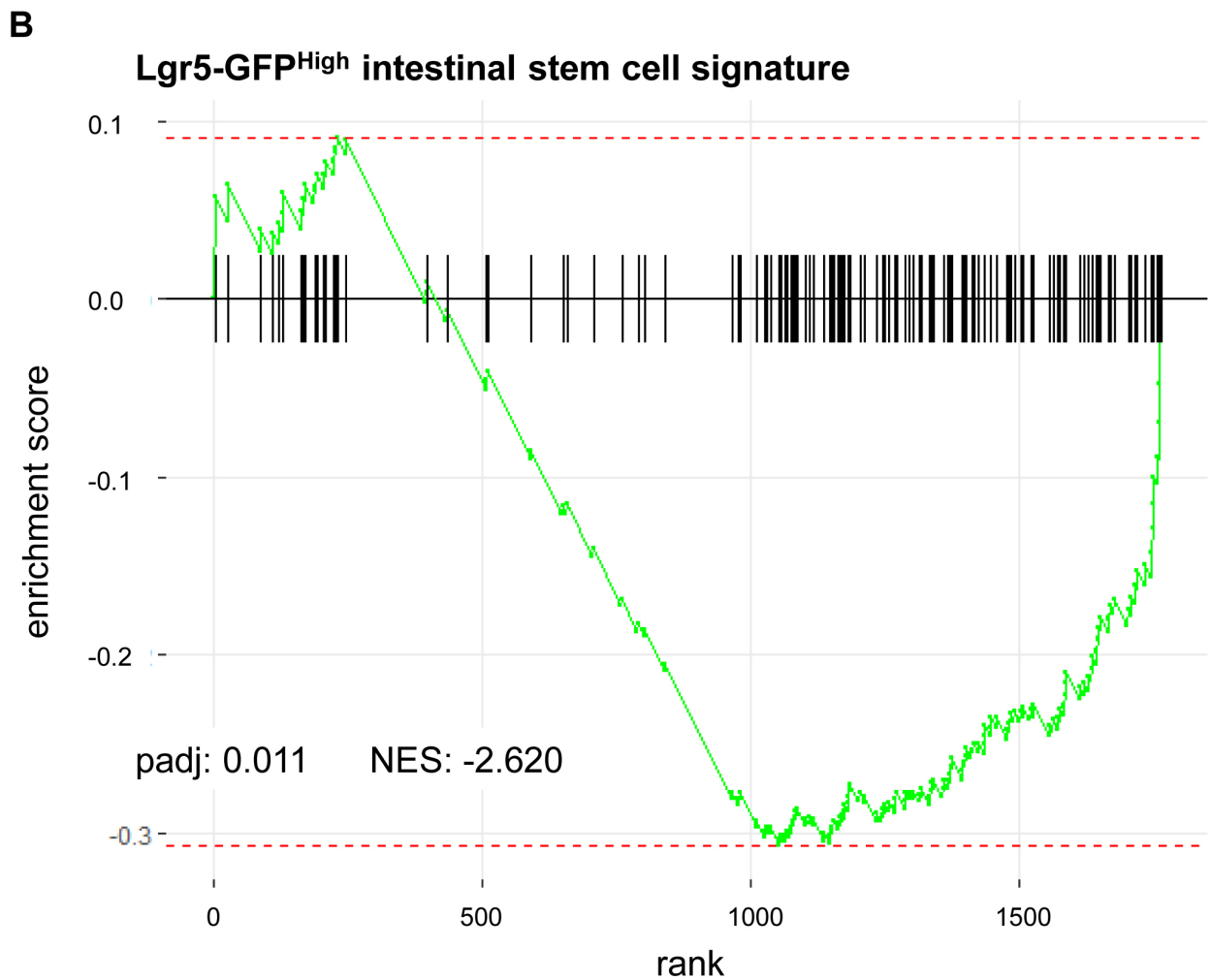
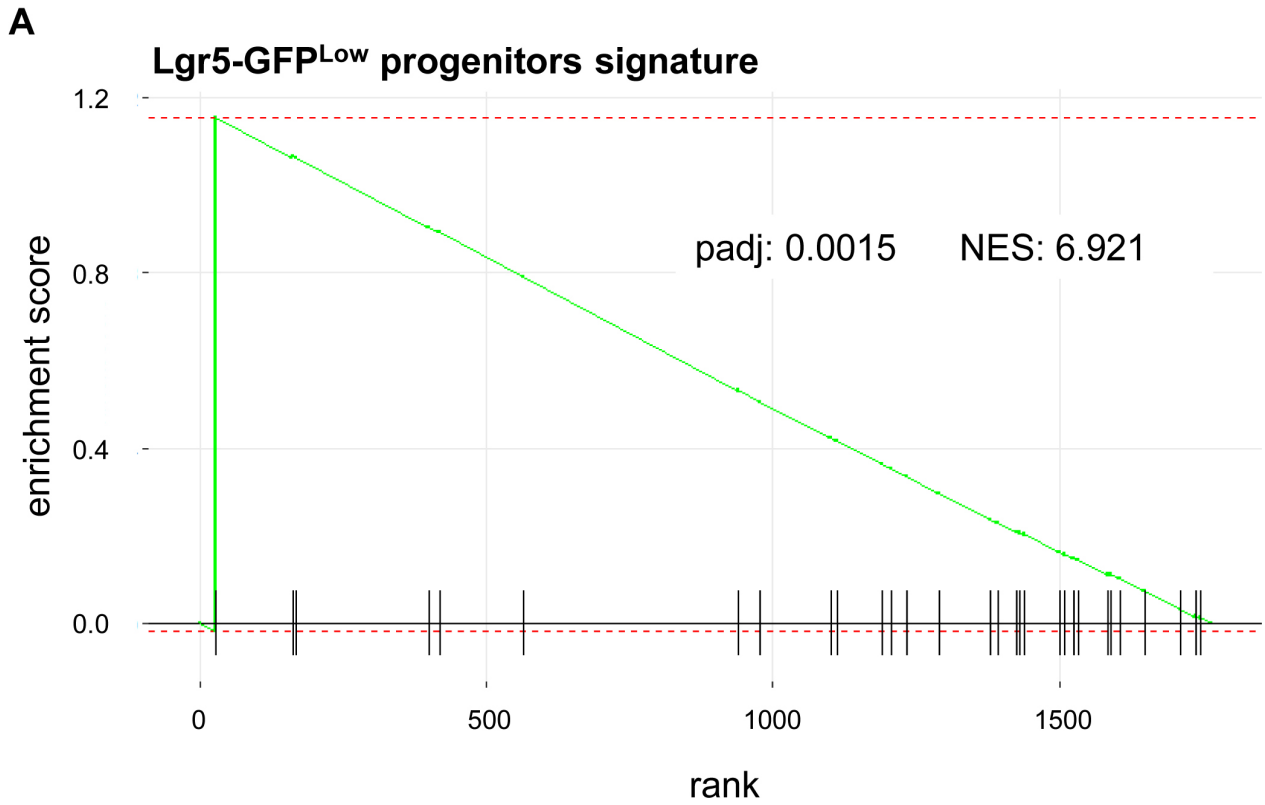
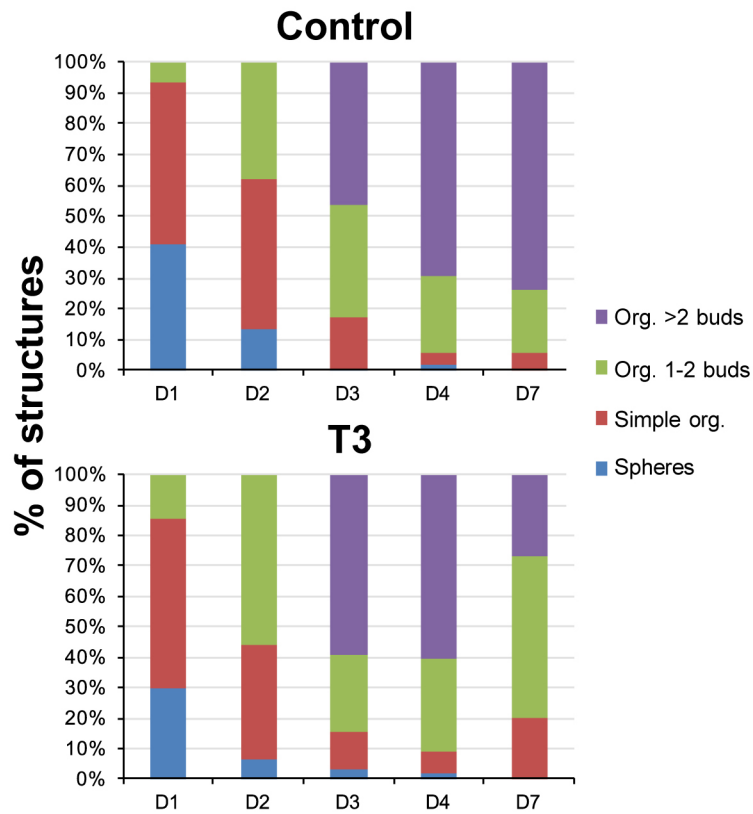


**Figure S3. Gene set enrichment analysis (GSEA).** Genes are ranked according to their differential expression between T3-treated and control organoids. Image showing the comparison of our DE genes and the genes characterizing progenitors (A) or the genes characterizing intestinal stem cell signature described in Munoz et al., 2012 (B). Black bars below each graph depict the position of common genes. NES: normalized enrichment score.



## Godart et al, Figure S4

**A**



**B**

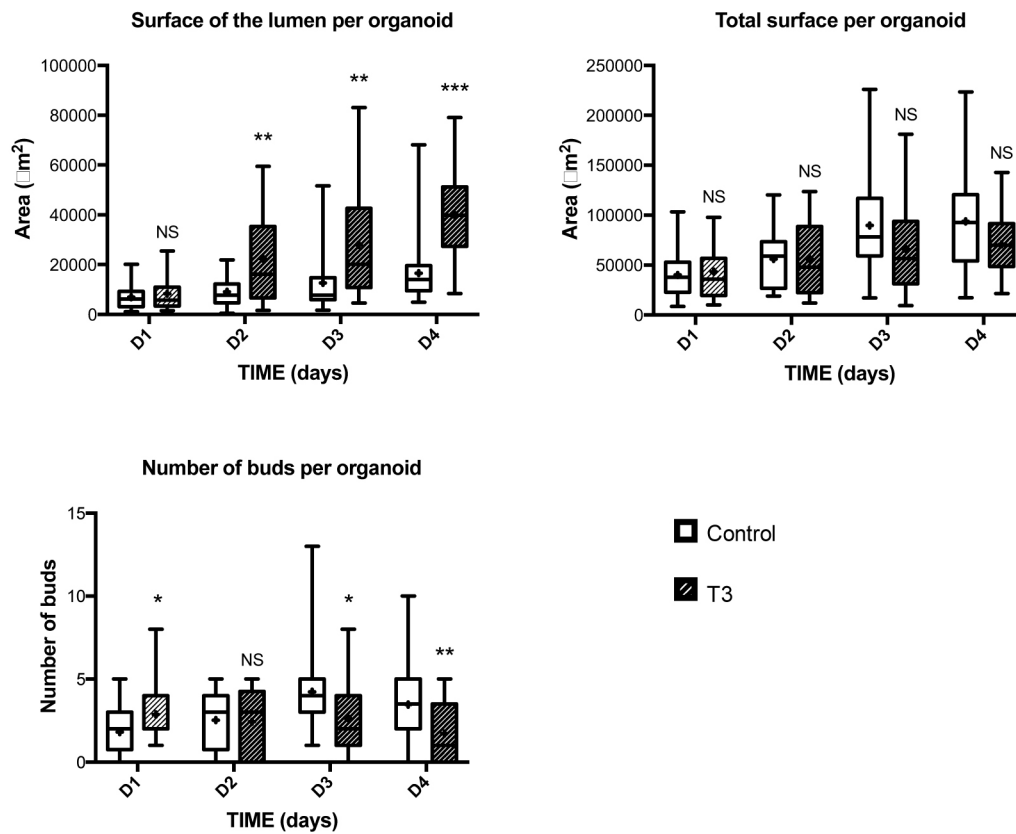


**Figure S4. Complementary growth properties and features of cultured crypts upon T3 treatment.** Crypts were prepared from *Lgr5*-EGFP intestine and maintained in culture for several days in the absence (Control) or presence of  $10^{-7}$  M T3, as indicated. A) Multilayered histograms represent the mean  $\pm$  SD,  $n = 6$ , of each counted structure in the cultured crypts in control or T3 condition. The percentage of spheres, simple organoids, 1-2 bud organoids and more complex organoids ( $> 2$  buds) was evaluated every day for 1 week. D, days in culture. B) Analysis of the lumen size, the total size and the number of buds per organoid was performed on representative images taken under the inverted microscope by using the ImageJ software. 30-50 organoid per day and per condition were analyzed. D, days in culture. NS, not significant; \*,  $P < 0.05$ , \*\*,  $P < 0.01$  and \*\*\*,  $P < 0.001$  compared to the respective control conditions.

Godart et al, Figure S5

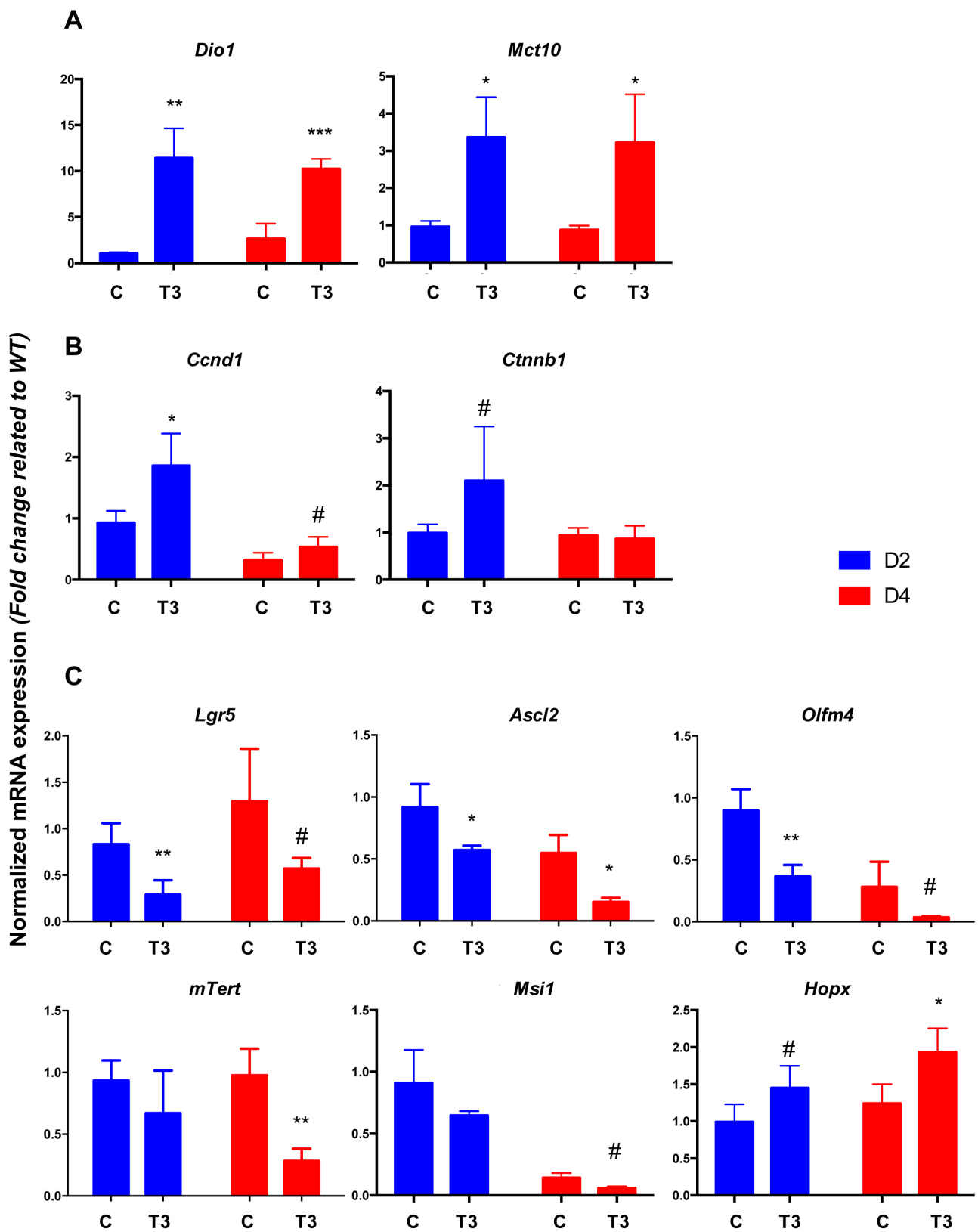




**Figure S5. Complementary molecular analyses of T3-treated organoids.** Replicated *Lgr5*-EGFP organoids were cultured in the absence (C, control) or presence of  $10^{-7}$  M T3 (T3), as indicated, for 2 (D2) and 4 days (D4). RT-qPCR experiments were performed to analyze the expression of TH metabolizing enzyme mRNA *Dio1* and transporter *Mct10* (A); *Ccnd1* (Cyclin D1) was used as proliferative marker and *Ctnnb1* ( $\beta$ -catenin) as a direct T3-target gene (B). C) Analysis of stem cell markers *Lgr5*, *Olfm4*, *Ascl2*, *mTert*, *Msi1* and *Hopx*. Histograms represent mean  $\pm$  SD, n = 4, after normalization against *Ppib*. The expression value of each gene is represented as fold change related to the control condition at D2. \*,  $P < 0.05$ , \*\*,  $P < 0.01$  and \*\*\*,  $P < 0.001$  compared to the respective control conditions. #: marginally significant compared to the respective control conditions.

## Godart et al, Figure S6

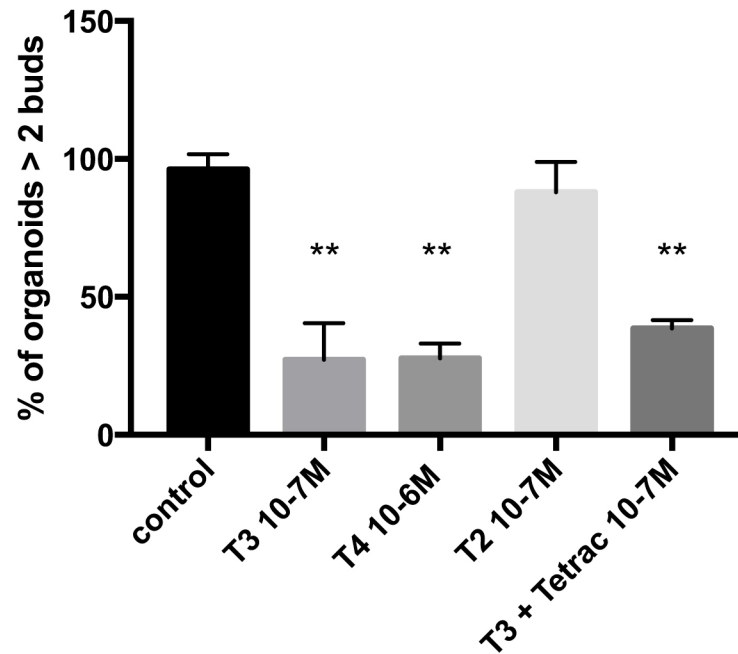
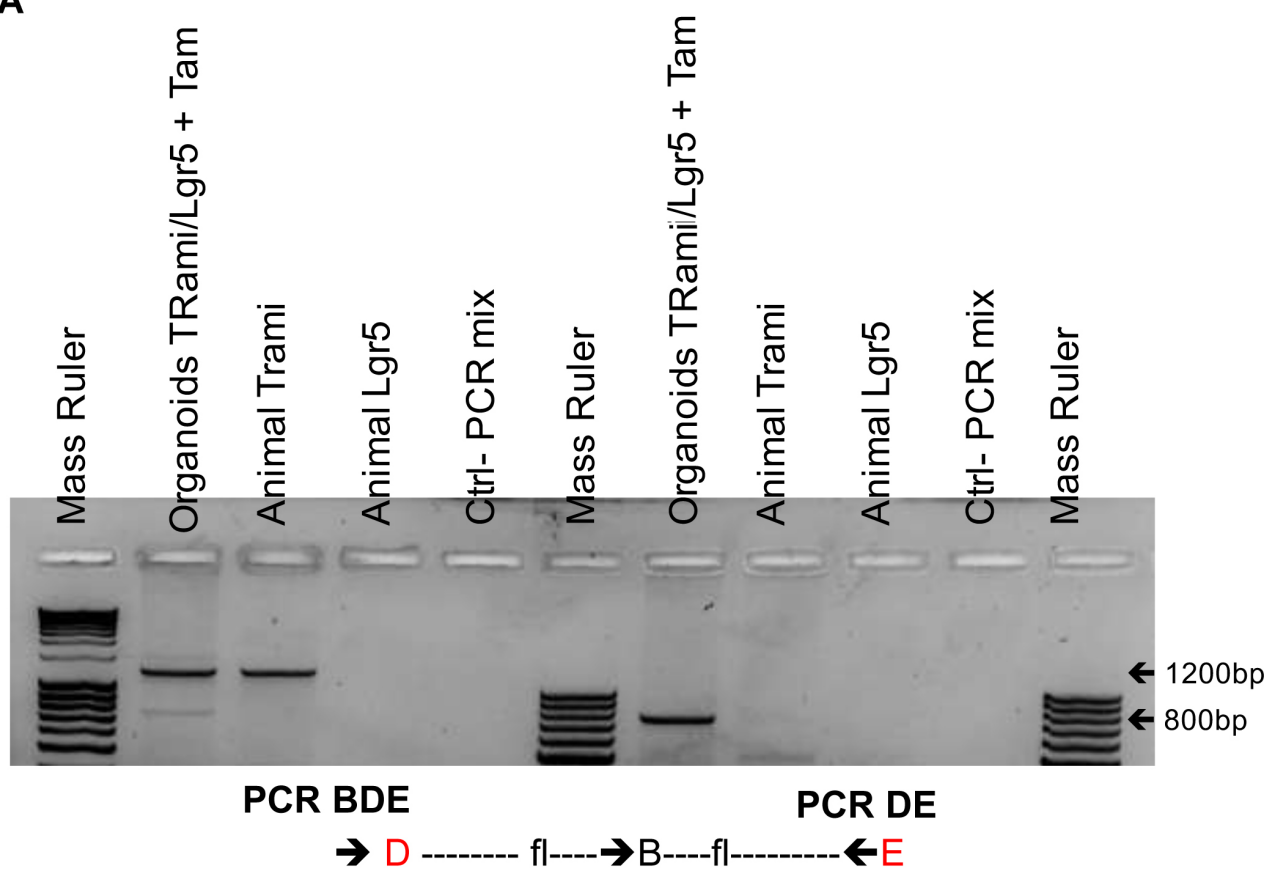


**Figure S6. Analysis of different TH-related molecules in organoids.** Replicated *Lgr5*-EGFP organoids were maintained in control, T3 ( $10^{-7}$  M), T4 ( $10^{-6}$  M), 3,3'-T2 ( $10^{-7}$  M) or T3 and Tetrac ( $10^{-7}$  M) (T3+Tetrac). The percentage of complex organoids (> 2 buds) was analyzed at D4. Histograms represent mean  $\pm$  SD, n = 6. \*\*,  $P < 0.01$  compared to the control or to the T2 condition.

## Godart et al, Figure S7

**A**



1200 bp : Non-recombined TRami allele

800 bp : Recombined TRami allele and expression of the TRami

**B**

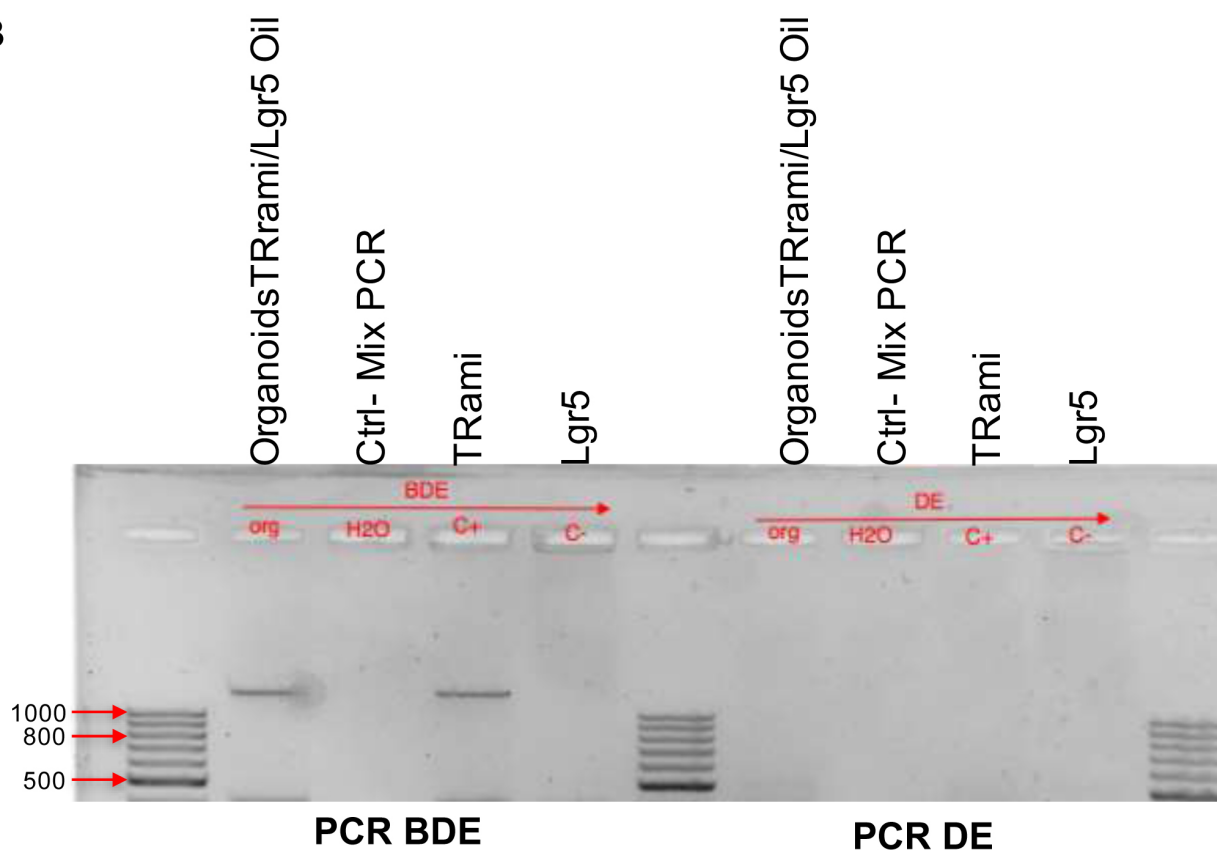


**Figure S7. Generation and validation of the TRami/*Lgr5*-EGFP/*Rosa*-Tomato animals and organoids.** PCR analysis on gDNA from triple transgenic TRami/*Lgr5*-EGFP/*Rosa*-Tomato organoids from previously tamoxifen- (A) or oil- (B) injected animals. Recombination of gDNA was evaluated after 4 days of culture and compared to controls (gDNA extracted from intestine of TRami or *Lgr5*-EGFP mice, PCR Mix). Combination of two (DE) or three (BDE) primers was used to amplify gDNA by PCR. In the presence of tamoxifen, 800 bp amplicons were detected, revealing the presence of the recombined TRami allele (A) whereas they were not detected when mice were injected with oil (B).



Godart et al, Figure S8

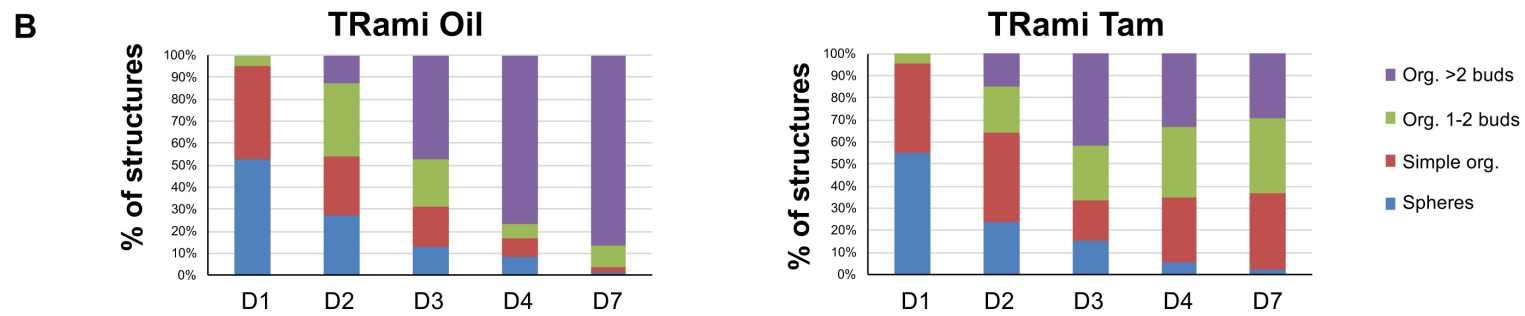
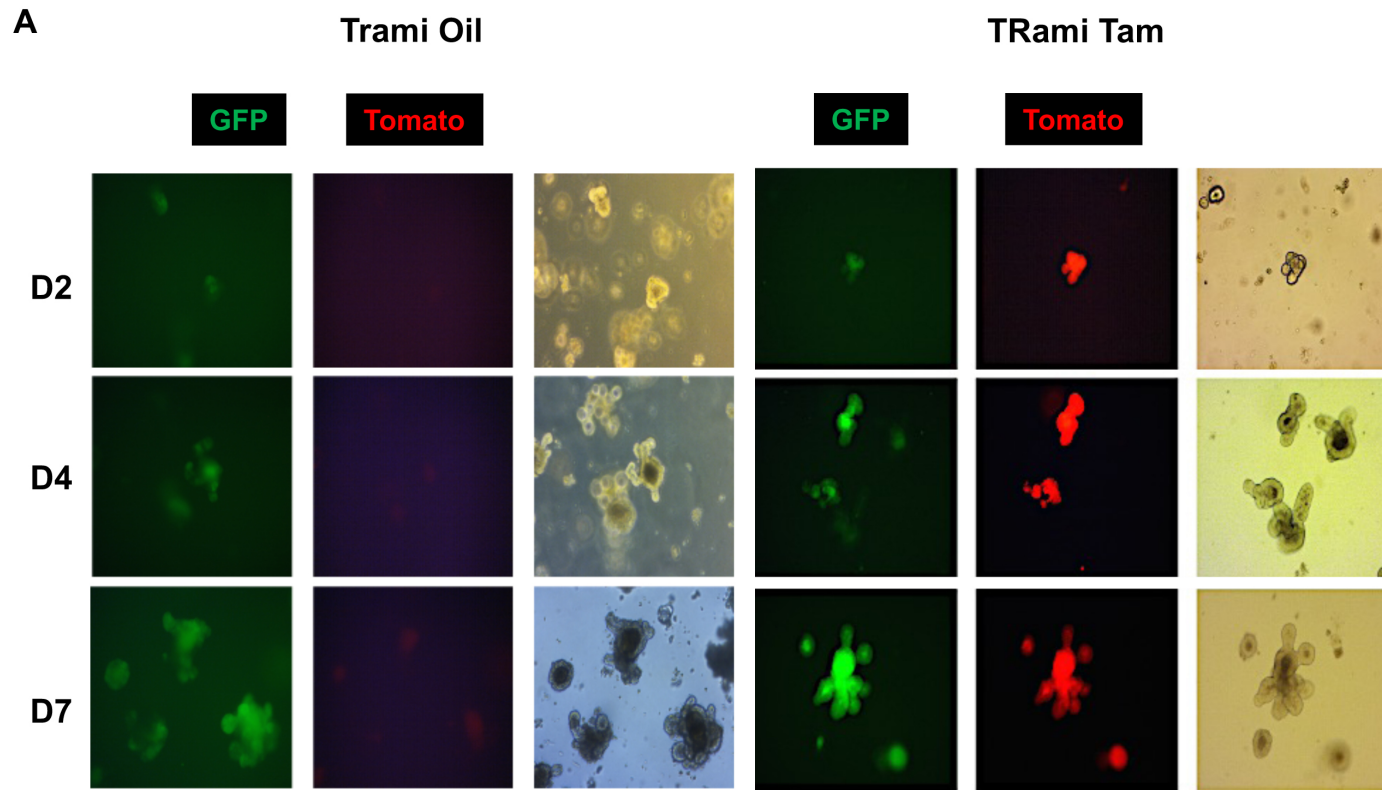


**Figure S8. Complementary phenotypic analysis of the TRami/*Lgr5*-EGFP/*Rosa*-Tomato organoids.** A) Live GFP and RFP fluorescence analysis of fresh triple transgenic organoids established from tamoxifen- or oil-injected mice, as indicated, and observed at D2, D4 and D7. D, days in culture. In TRami/*Lgr5*-EGFP/*Rosa*-Tomato animals, tamoxifen injections induced deletion of floxed sites enabling the expression of the Tomato protein (red fluorescence) as well as of the TRami allele. No recombination could be observed in organoids established from oil-treated animals, confirmed by the absence of Tomato signal. Left: GFP, Middle: Tomato, Right: Brightfield. Pictures have been taken under an inverted microscope at the indicated days after the start of the culture, and are representative of two independent experiments, each conducted on six replicates (Bar = 50  $\mu$ m). B) Multilayered histograms represent the mean  $\pm$  SD, n = 6, of each counted structure in the cultured crypts in oil or Tam condition. The percentage of spheres, simple organoids, 1-2 bud organoids and more complex organoids (> 2 buds) was evaluated every day for 1 week. D, days in culture.

## Godart et al, Figure S9

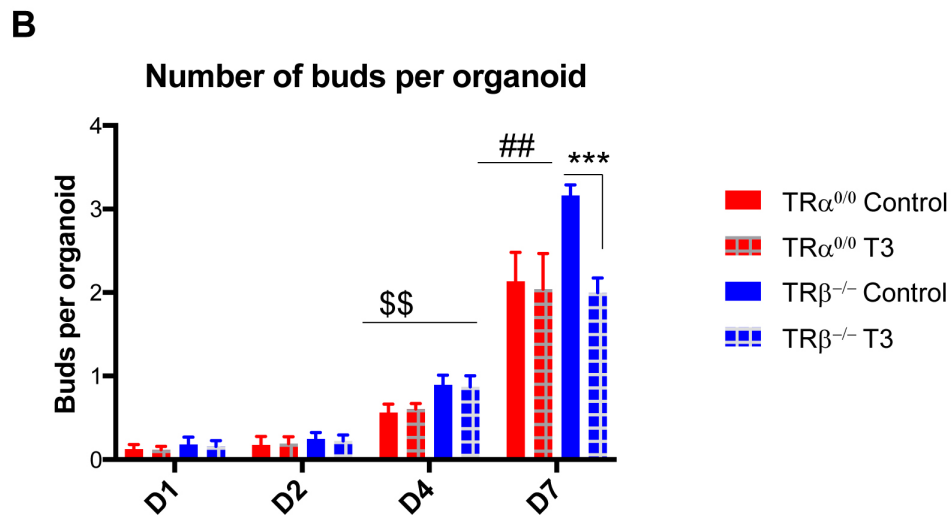
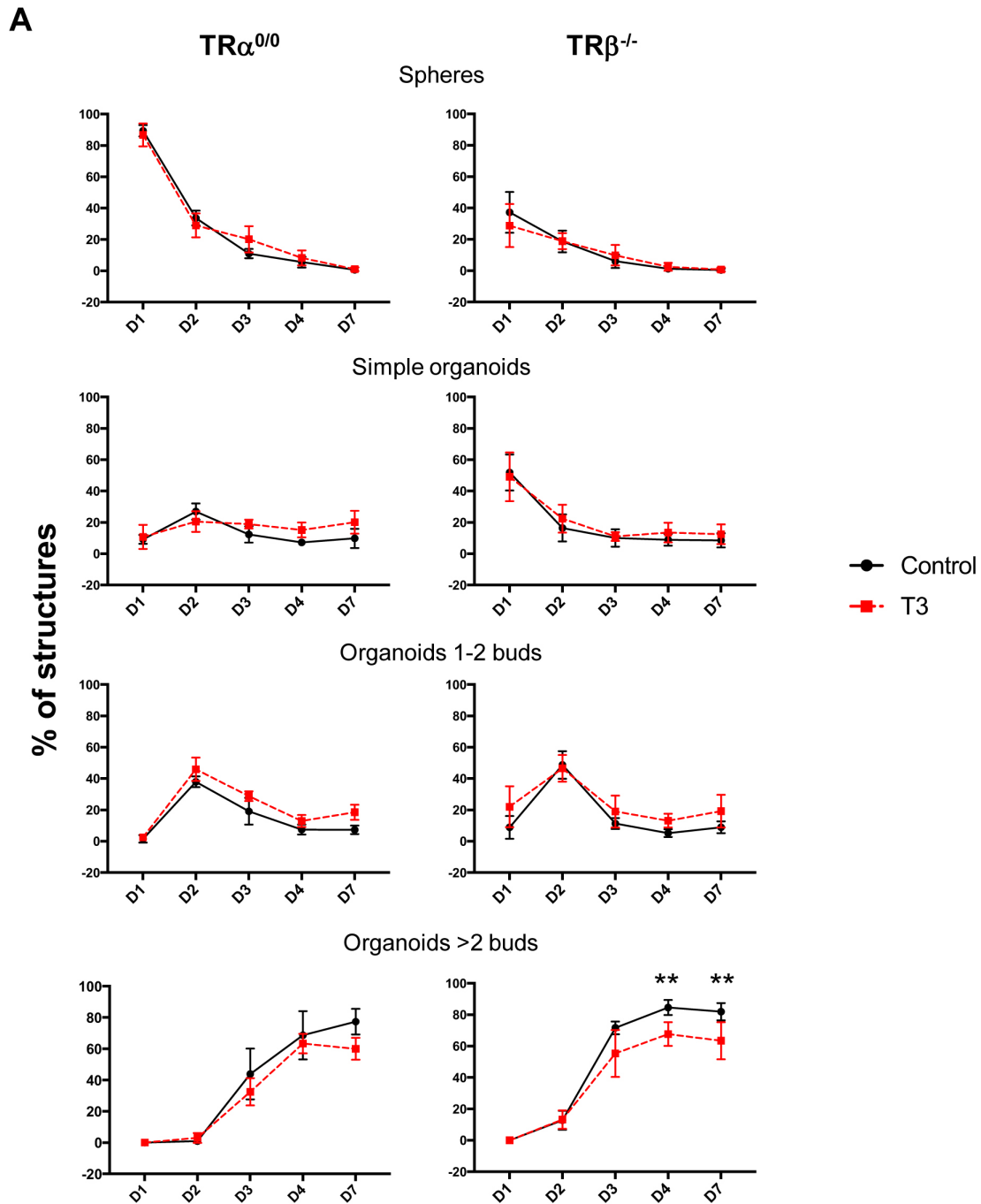


**Figure S9. Complementary analyses on organoids from TR $\alpha$ <sup>0/0</sup> and TR $\beta$ <sup>-/-</sup> mice.** A) Crypts were prepared from TR $\alpha$ <sup>0/0</sup> and TR $\beta$ <sup>-/-</sup> intestine and maintained in culture for several days in the absence (Control) or presence of 10<sup>-7</sup> M T3, as indicated. The number of simple structures (spheres) or organoids of increasing complexity (1 or 2 buds, more than 2 buds) in control and T3 condition, as indicated, were scored under the inverted microscope during seven days of culture. Graph lines represent the mean  $\pm$  SD, n = 6, of each structure counted in the cultures from different genotypes and conditions. \*\*, *P* < 0.01 compared to the respective control condition. B) The number of buddings per organoid was scored at different time points in cultured organoids of different genotypes in control and T3 conditions, as indicated. Histograms represent mean  $\pm$  SD, n = 20. \$\$, *P* < 0.01 compared to TR $\beta$ <sup>-/-</sup> control or T3 conditions; ##, *P* < 0.01 compared to the TR $\beta$ <sup>-/-</sup> control condition; \*\*, *P* < 0.01 compared to the control condition of the same genotype.



## Godart et al, Figure S10

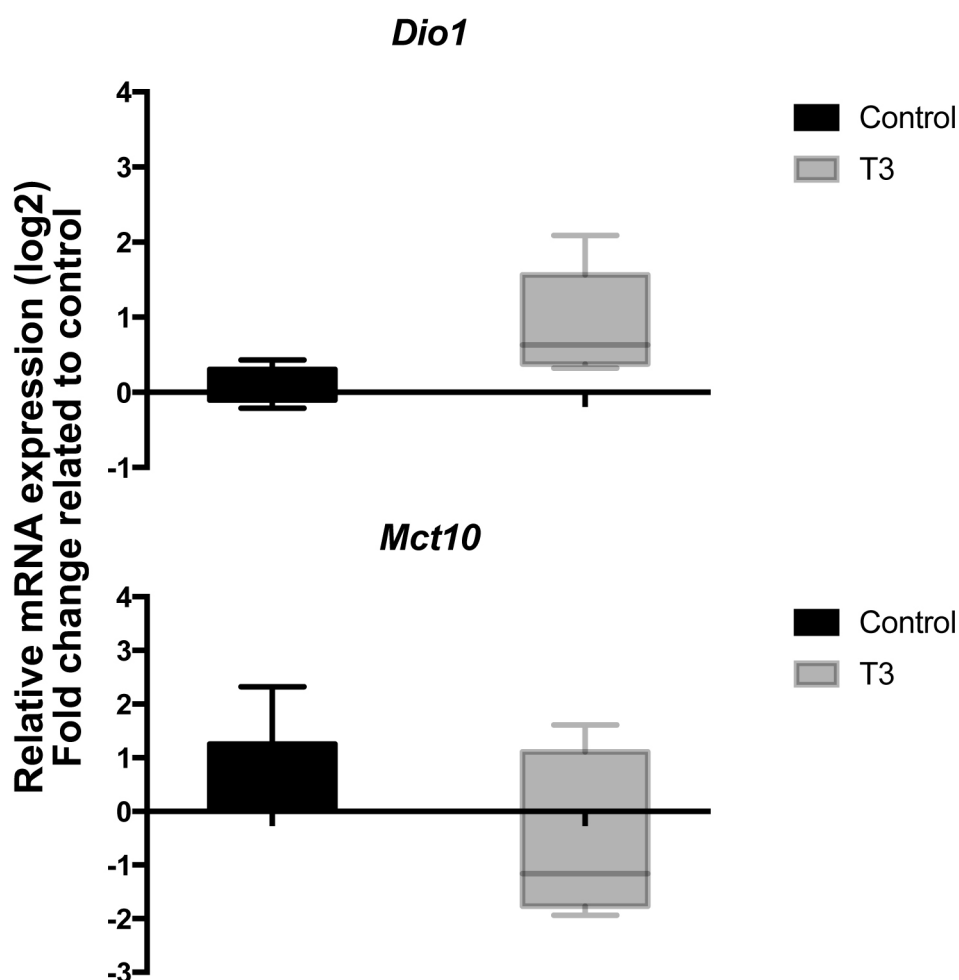
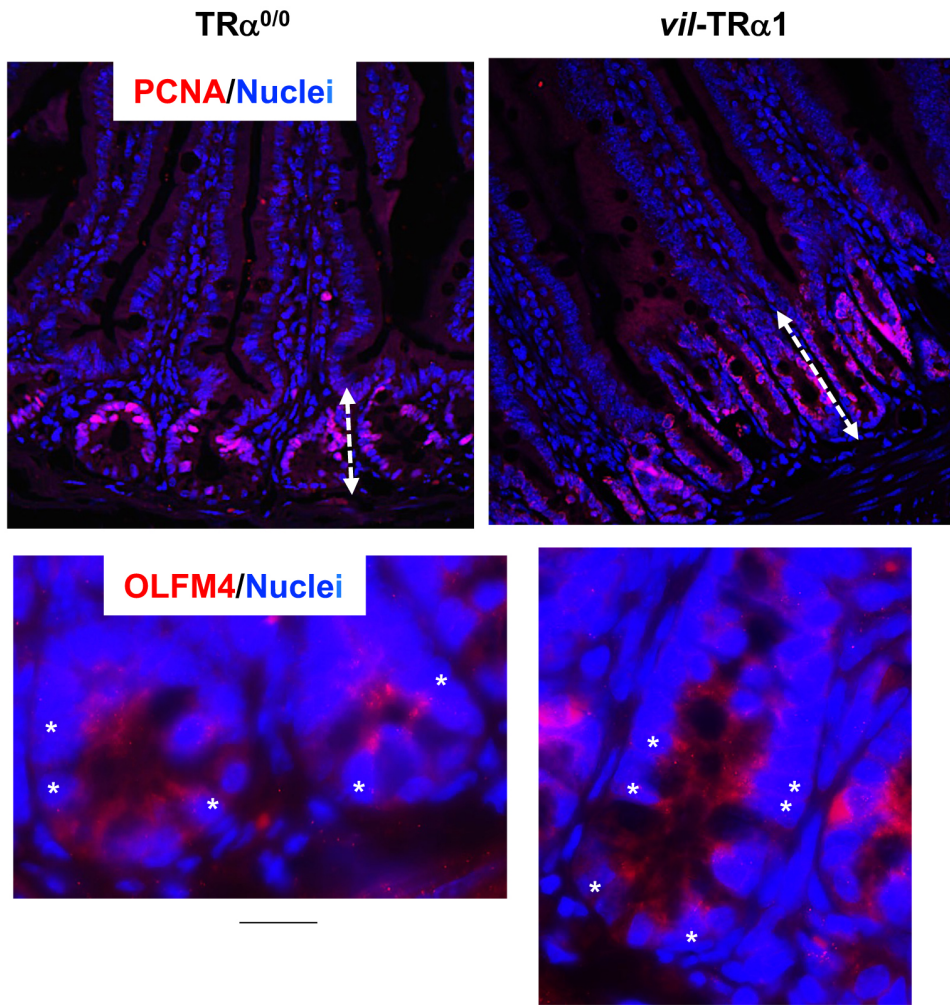


**Figure S10. Effect of T3 treatment *in vivo* on *Dio1* and *Mct10* mRNA expression.** A) RT-qPCR experiments to analyze the expression of TH metabolizing enzyme *Dio1* and transporter *Mct10* mRNAs. The study was performed on RNA extracted from the distal small intestinal mucosa. Boxplots show the distribution of data and the mean  $\pm$  SD,  $n = 6$ , after normalization against *Ppib*. Data are represented as fold change relative to the control condition.

## Godart et al, Figure S11

A



B

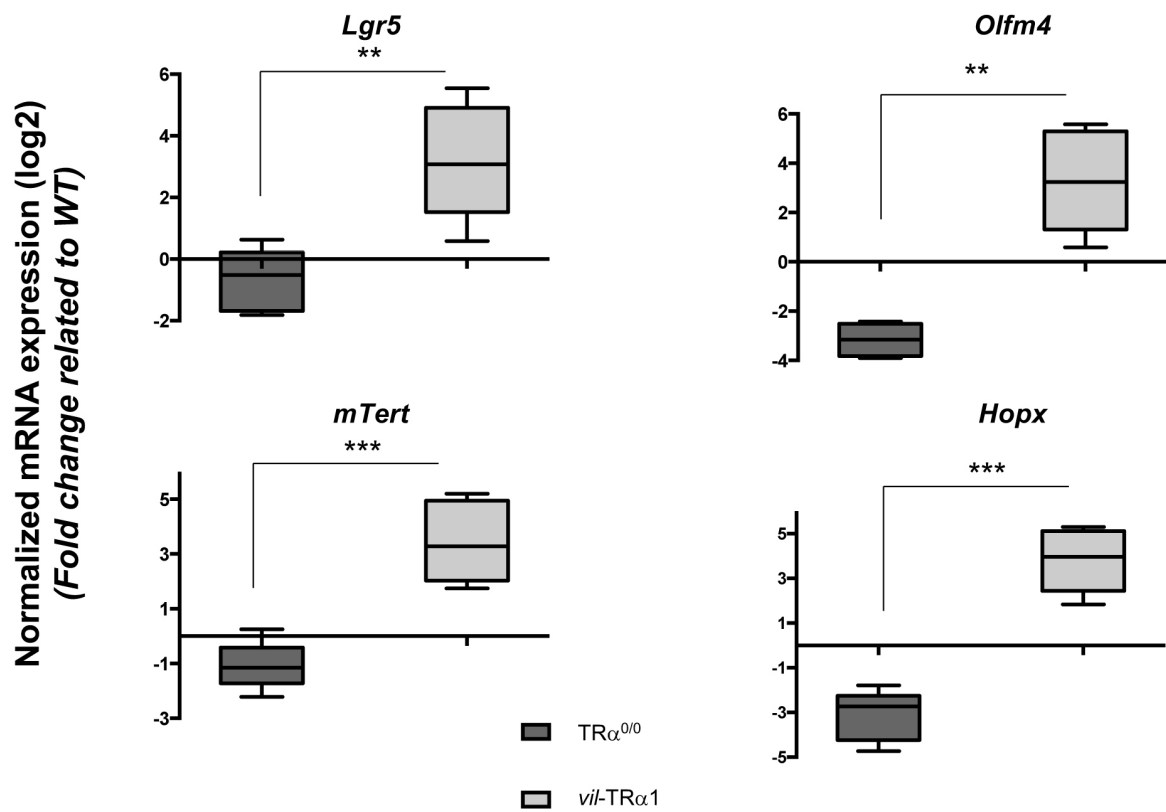


**Figure S11. TR $\alpha$ 1 modulation *in vivo* affects intestinal stem cells.** A) Analysis of PCNA-positive proliferating cells (upper panels) or OLFM4-positive stem cells (lower panels) in distal small intestinal sections from TR $\alpha$ <sup>0/0</sup> and *vil*-TR 1 animals, representing models of constitutive TR $\alpha$ -knockout and TR $\alpha$ 1-targeted overexpression, respectively (Gauthier et al, 2001; Kress et al, 2010). The images show merged PCNA or OLFM4 (red) and nuclear staining (blue). Pictures are representative of three different animals per condition. Bar PCNA = 10  $\mu$ m; bar OLFM4 = 5  $\mu$ m. The white dotted double-arrow indicates the PCNA-positive crypt length; white asterisks point to OLFM4-positive cells. B) RT-qPCR analysis on stem cell markers *Lgr5*, *Olfm4*, *Hopx* and *mTert*. The study was performed on RNA extracted from the distal small intestinal mucosa. Boxplots show the distribution of data and the mean  $\pm$  SD, n = 6, after normalization against *Ppib*. Data are represented as fold change relative to the control condition.

**Table S1. Differentially-expressed genes between T3-treated and control organoids.**

[Click here to download Table S1](#)

**Table S2. Comparative analyses between T3-treated and control organoids vs SC or progenitor gene signatures.**

[Click here to download Table S2](#)

**Table S3: Genes specifically expressed in Progenitor cells.**

[Click here to download Table S3](#)



**Table S4. Comparative analyses between T3-treated and control organoids vs genes described in Kress et al., 2009.**

Gene Symbol	Kress 2009	RNA-seq 2019	Function
Acot1	down	down	Palmitoyl-CoA hydrolase activity; hydrolase activity
Acss1	down	down	Acetyl-CoA biosynthetic process; metabolic process
Adh1	down	down	Retinoid metabolic process; alcohol dehydrogenase (NAD) activity; retinol dehydrogenase activity
Akr1c13	down	down	Xenobiotic metabolic process; oxidation-reduction process
Aldh1a1	down	down	Retinol metabolic process; retinoic acid metabolic process; 9-cis-retinoic acid biosynthetic process
Aldh1a7	down	down	Retinoic acid metabolic process
Amn	down	down	Cell adhesion/extracellular matrix
Apobec1	up	up	Nucleic acid metabolism; mRNA processing
Apobec3	up	up	Nucleic acid metabolism
Armcx1	down	down	Membrane proteins/transporters
Atp13a3	down	down	Cation transport; cellular calcium ion homeostasis
Bmp7	down	down	Transforming growth factor beta receptor binding; growth factor activity; BMP receptor binding
Cat	down	down	Stress and apoptosis
Cldn8	down	down	Cell adhesion/extracellular matrix
Cxcr5	down	down	Transcriptional regulation
Cytc	up	up	Metabolism; cytochrome c oxidase complex activity
Dab1	down	down	Cell adhesion/extracellular matrix
Dhrs7	up	up	Metabolic process; oxidation-reduction process
Dock5	up	up	Cell cycle control/proliferation
Elovl6	up	up	Fatty acid elongase activity; transferase activity
<b>Fgf1</b>	<b>down</b>	<b>up</b>	<b>Intestinal crypt formation; response to irradiation</b>
Faah	down	down	Fatty acid catabolic process
Fmo5	down	down	Oxidoreductase activity and NADP binding
Fos	up	up	Proto-Oncogene, Transcription Factor
<b>Gcnt2</b>	<b>down</b>	<b>up</b>	<b>Remodeling glycans; barrier function; regulating Muc expression</b>
Gng10	up	up	G protein, involved as a modulator or transducer in various transmembrane signaling systems
Gp1bb	up	up	Transmembrane signaling receptor activity
Gpx2	up	up	Detoxification of Reactive Oxygen Species
Gsta1	up	up	Glutathione transferase activity
Gstm4	down	down	Glutathione transferase activity
Higd1a	up	up	Mitochondrial respiratory chain that catalyzes the reduction of oxygen
Hmgcs2	down	down	Mitochondrial enzyme that catalyzes the first reaction of ketogenesis
ldh3a	up	up	Pyruvate metabolism and Citric Acid (TCA) cycle
Kcne3	up	up	Voltage-gated potassium channel activity
Klf9	up	up	Regulation of transcription; cellular response to thyroid hormone stimulus
Lbp	up	up	Liver development; lipid transport; inflammatory response
Letm1	up	up	Protein binding; metal ion binding
Marcks11	down	down	Positive regulation of cell proliferation
Nnt	dwn	down	NADPH regeneration; proton transport; cell redox homeostasis
<b>Notch1</b>	<b>up</b>	<b>down</b>	<b>Stem cell biology; activation in enterocyte progenitor</b>
Psmb8	up	up	Threonine-type endopeptidase activity
Pxmp4	down	down	Peroxisomal membrane; protein binding
Sesn1	up	up	Regulation of protein kinase B signaling; regulation of response to reactive oxygen species
Sh3bgr	up	up	SH3 domain binding
Slc13a1	up	up	Sodium-sulfate symporter activity
Stard5	down	down	Lipid transport; lipid binding; cholesterol binding; bile acid binding
Steap1	up	up	Ion transport; oxidoreductase activity
Tcf23	down	down	Protein dimerization activity
Tcf4	down	down	Transcription factor activity
Tgfb1	up	up	Collagen binding; cell adhesion molecule
Tlr3	up	up	Toll-like receptor signaling pathway; involved in immune response
Tnfrsf14	up	up	Tumor necrosis factor-activated receptor activity; protein binding
Ttr	down	down	Hormone binding; protein binding; thyroid hormone binding
Upp1	up	up	Catalytic activity; uridine phosphorylase activity; transferase activity

**Table S5: Expression of *Thra* gene in different crypt populations.**

<b>GSE25109 - Stem Cells - Present Genes*</b>		<b>GSE25109 - Paneth Cells - Present Genes*</b>		<i>* Present Gene = flagged as "P" in 4/4 samples</i>	
<b>GeneName</b>		<b>GeneName</b>			
Thra		Thra			
<b>GSE23672 -GFPHigh - Present Genes*</b>		<b>GSE23672 - Low - Present Genes*</b>		<i>* Present Gene = flagged as "P" in 4/4 samples</i>	
<b>GeneName</b>		<b>GeneName</b>			
Thra		Thra			
<b>GSE25109 - Differential analysis - Stem Cells vs. Paneth Cells (Fold-Change &gt; 1.5 &amp; Pvalue &lt; 0.05)</b>					
<b>GeneName</b>	<b>SystematicName</b>	<b>Fold-Change (StemCells vs PanethCells)</b>	<b>P-value (StemCells vs PanethCells)</b>	<b>Description</b>	
Thra	NM_178060	2.20145311274614	0.00459508961922441	ref Mus musculus thyroid hormone receptor alpha (Thra), mRNA [NM_178060]	
<b>GSE23672 - Differential analysis - High vs. Low (Fold-Change &gt; 1.5 &amp; Pvalue &lt; 0.05)</b>					
<b>GeneName</b>	<b>SystematicName</b>	<b>Fold-Change (High vs Low)</b>	<b>P-value (High vs Low)</b>	<b>Description</b>	
Thra	NM_178060	1.60923971813349	0.0129884032909439	ref Mus musculus thyroid hormone receptor alpha (Thra), mRNA [NM_178060]	

Table S6: oligonucleotides used for RTqPCR studies		
Gene symbol	Category	Sequence (5'-3') forward / reverse
Ppib	Housekeeping gene	CAC CAA TGG CTC ACA GTT CTT
		ATG ACA TCC TTC AGT GGC TTG
Dio1	Thyroid hormone deiodinase selenoenzyme	AGA GAG CCA GAT TCC TGT GC
		GCT TGT AGG AAC CAT AGG CAT TGG
Mct10	Thyroid hormone transporter	CAA GGA CGA TGA CAA CAT GG
		GTC CGT GAA GAC ACT CAC GA
Lgr5	Active stem cell marker	GAC AAT GCT CTC ACA GAC
		GGA GTG GAT TCT ATT ATT ATG G
Ascl2	Active stem cell marker	CCT ATG CCT TAC CCA TGC T
		TTT CCA AGT CCT GAT GCT G
mTert	Facultative stem cell marker	GCA GGT GAA CAG CCT CCA GAC AG
		TCC TAA CAC GCT GGT CAA AGG GAA GC
Olfm4	Active stem cell marker	CTG TGG GCA ATT TAT GCA ACT
		CAG ATG GCT TGT ACT GCT TGG
Msi1	Active and reserve stem cell marker	ATG CTG GGT ATT GGG ATG CT
		CGG GGA ACT GGT TGT AA
Hopx	Facultative stem cell marker	CAT CCT TAG TCA GAC GCG CA
		AGG CAA GCC TTC TGA CCG C
Jag1	Voie Notch, TR $\alpha$ 1 direct target gene	ACCAAGCTCAAGATCAAAAA
		TTTATTGCCAGGAACAACAC
Ctnnb1	Voie Wnt, TR $\alpha$ 1 direct target gene	AGCCGAGATGGCCCAGAAT
		AAGGGCAAGGTTTCGAATCAA
Ccnd1	Cell cycle, cell proliferation	CAGAGGCGGATGAGAACAAGT
		GCGGTAGCAGGAGAGGAAG

<b>Table S7: antibodies used</b>			
<b>Western blot</b>			
<b>Antigen</b>	<b>Brand, Ref</b>	<b>Species</b>	<b>Dilution</b>
CASPASE 3	Cell signaling, 9661	Rabbit	1/1000
PHOSPHO H3	Santa cruz, sc-10809	Rabbit	1/500
$\beta$ -ACTIN	Sigma, A5316	Mouse	1/10000
Secondary antibody HRP-conjugated	Promega, W4011	Anti Rabbit	1/10000
	Promega, W4021	Anti Mouse	1/10000
<b>Immunolabeling</b>			
GFP	Millipore, AB16901	Chicken	1/500
CASPASE 3	Cell signaling, 9661	Rabbit	1/100
CHGA	Zymed, 18-0094	Rabbit	1/500
LYZ	Abcam, ab108508	Mouse	1/500
MUC2	Santa Cruz, sc-15334	Rabbit	1/100
KI67	Abcam, ab16667	Rabbit	1/200
OLFM4	Abcam, ab85046	Rabbit	1/200
PCNA	Dako, M0879	Mouse	1/1000
Secondary antibody Fluorescence-conjugated	Molecular Probes, A10042	Anti Rabbit	1/1000
	Molecular Probes, A11039	Anti Chicken	1/500
	Molecular Probes, A11004	Anti Mouse	1/1000